frontiers in Molecular Neuroscience

ORIGINAL RESEARCH
published: 02 November 2020
doi: 10.3389/fnmol.2020.552073

The Interplay Between Beta-Amyloid 1–42 ($A\beta_{1–42}$)-Induced Hippocampal Inflammatory Response, p-tau, Vascular Pathology, and Their Synergistic Contributions to Neuronal Death and Behavioral Deficits

*Beatriz Calvo-Flores Guzmán[1], Tessa Elizabeth Chaffey[1], Thulani Hansika Palpagama[1], Sarah Waters[1], Jordi Boix[2], Warren Perry Tate[3], Katie Peppercorn[3], Michael Dragunow[4], Henry John Waldvogel[1], Richard Lewis Maxwell Faull[1] and Andrea Kwakowsky[1]**

[1]Centre for Brain Research, Department of Anatomy and Medical Imaging, Faculty of Medical and Health Sciences, University of Auckland, Auckland, New Zealand, [2]Centre for Brain Research, NeuroDiscovery Behavioural Unit, Faculty of Medical and Health Sciences, University of Auckland, Auckland, New Zealand, [3]Department of Biochemistry, University of Otago, Dunedin, New Zealand, [4]Centre for Brain Research, Department of Pharmacology, Faculty of Medical and Health Sciences, University of Auckland, Auckland, New Zealand

OPEN ACCESS

Edited by:
Robert A. Nichols,
University of Hawaii at Manoa,
United States

Reviewed by:
Fernando Peña-Ortega,
National Autonomous University of Mexico, Mexico
Annakaisa Haapasalo,
University of Eastern Finland, Finland

***Correspondence:**
Andrea Kwakowsky
a.kwakowsky@auckland.ac.nz

Received: 15 April 2020
Accepted: 22 September 2020
Published: 02 November 2020

Citation:
Calvo-Flores Guzmán B, Chaffey TE, Palpagama TH, Waters S, Boix J, Tate WP, Peppercorn K, Dragunow M, Waldvogel HJ, Faull RLM and Kwakowsky A (2020) The Interplay Between Beta-Amyloid 1–42 ($A\beta_{1–42}$)-Induced Hippocampal Inflammatory Response, p-tau, Vascular Pathology, and Their Synergistic Contributions to Neuronal Death and Behavioral Deficits. Front. Mol. Neurosci. 13:552073. doi: 10.3389/fnmol.2020.552073

Alzheimer's disease (AD), the most common chronic neurodegenerative disorder, has complex neuropathology. The principal neuropathological hallmarks of the disease are the deposition of extracellular β-amyloid (Aβ) plaques and neurofibrillary tangles (NFTs) comprised of hyperphosphorylated tau (p-tau) protein. These changes occur with neuroinflammation, a compromised blood-brain barrier (BBB) integrity, and neuronal synaptic dysfunction, all of which ultimately lead to neuronal cell loss and cognitive deficits in AD. $A\beta_{1–42}$ was stereotaxically administered bilaterally into the CA1 region of the hippocampi of 18-month-old male C57BL/6 mice. This study aimed to characterize, utilizing immunohistochemistry and behavioral testing, the spatial and temporal effects of $A\beta_{1–42}$ on a broad set of parameters characteristic of AD: p-tau, neuroinflammation, vascular pathology, pyramidal cell survival, and behavior. Three days after $A\beta_{1–42}$ injection and

Abbreviations: Aβ, β-amyloid; ACSF, artificial cerebrospinal fluid; AD, Alzheimer's disease; BBB, blood-brain barrier; CA 1, cornu ammonis region 1; CX3CR1, CX3C chemokine receptor 1; DR, discrimination ratio; E/I, excitatory/inhibitory; FPLC, fast protein liquid chromatography; IBA-1, ionized calcium-binding adaptor molecule 1; ICV, intracerebroventricular; LTP, long-term potentiation; $GABA_A$Rs, GABA type (A) receptors; GFAP, glial fibrillary acidic protein; IP-10, interferon-inducible protein 10; MAPT, microtubule-associated protein Tau; MBP, maltose-binding protein; MCP-1, monocyte chemotactic protein-1; MWM, Morris water maze; NC, naïve control; NeuN, neuronal nuclei; NFTs, neurofibrillary tangles; NOA, novel object alteration; NOR, novel object recognition; NVU, neurovascular unit; OM, O-maze; PBST, phosphate-buffered saline with Tween-20; PFA, paraformaldehyde; PC, pyramidal cell; PMSF, phenylmethanesulfonyl fluoride; RT, room temperature; Str, stratum; TBS, Tris-buffered saline; TBST, tris-buffered saline Tween-20; TFA, trifluoroacetic acid; Tg, transgenic; TGF-β1, transforming growth factor-β 1; TTB, 0.05 M TBS/0.3% Triton/0.25% BSA; YM, Y-maze; α-SMA, alpha-smooth muscle actin.

before significant neuronal cell loss was detected, acute neuroinflammatory and vascular responses were observed. These responses included the up-regulation of glial fibrillary acidic protein (GFAP), cell adhesion molecule-1 (PECAM-1, also known as CD31), fibrinogen labeling, and an increased number of activated astrocytes and microglia in the CA1 region of the hippocampus. From day 7, there was significant pyramidal cell loss in the CA1 region of the hippocampus, and by 30 days, significant localized up-regulation of p-tau, GFAP, Iba-1, CD31, and alpha-smooth muscle actin (α-SMA) in the $A\beta_{1-42}$-injected mice compared with controls. These molecular changes in $A\beta_{1-42}$-injected mice were accompanied by cognitive deterioration, as demonstrated by long-term spatial memory impairment. This study is reporting a comprehensive examination of a complex set of parameters associated with intrahippocampal administration of $A\beta_{1-42}$ in mice, their spatiotemporal interactions and combined contribution to the disease progression. We show that a single Aβ injection can reproduce aspects of the inflammatory, vascular, and p-tau induced pathology occurring in the AD human brain that lead to cognitive deficits.

Keywords: Alzheiemer's disease, β-amyloid, tau phosphorylation, cognition, neuroinflamamation

INTRODUCTION

Alzheimer's disease (AD) is a progressive neurodegenerative disorder characterized by a widespread loss of neuronal synapses and spines, the presence of intracellular neurofibrillary tangles (NFTs), and extracellular β-amyloid (Aβ) plaques (Huang and Mucke, 2012; Brun and Englun, 1981). During the last two decades, these features have been incorporated into the amyloid cascade hypothesis (Eric et al., 2011). Today, the successive downstream events occurring as a result of Aβ aggregation and spread represent a key thread of the hypotheses to explain the pathology observed in AD (Hardy and Selkoe, 2002). Despite a large number of clinical trials, there is still currently no effective treatment to prevent, significantly delay, or ameliorate the debilitating symptoms of AD. This is largely due to our limited understanding of the connecting factors underlying the disease, as well as the poor translation of promising treatment options derived from animal models to human clinical trials (Franco and Cedazo-Minguez, 2014; Souchet et al., 2018). With the prevalence of AD increasing alarmingly, it is crucial to develop animal models that more closely mimic the pathological and clinical symptoms of human AD. Importantly, such a model has to be well characterized to document its limitations (Drummond and Wisniewski, 2017) and to determine whether it might effectively support drug screening for the development of novel and effective treatments for AD.

A rising concentration of Aβ in the brain is a critical factor in the development of late-onset sporadic AD, playing a key role in triggering the "amyloid cascade." Although transgenic models, such as amyloid protein precursor (APP)- and presenilin-1 (PS-1)-overexpressing models are known to be useful in the study of genetic aspects of early-onset AD (Ohno et al., 2004, 2007), the late-onset sporadic form of the disease, that accounts for approximately 90% of all cases (Bekris et al., 2010), requires unique approaches to model this form of AD. Growing evidence indicates that Aβ-injected rodent models of AD might closely mimic the main neuropathological symptoms present in AD patients when concentrations of Aβ are increasing (Puzzo et al., 2014; Kwakowsky et al., 2016; Facchinetti et al., 2018; Baluchnejadmojara et al., 2019; Mudò et al., 2019; Yeung et al., 2020a,b). With this model, many aspects of AD-related pathology post-Aβ-injection and their link to the cognitive deficits are not fully characterized. Some of the key events occurring in the AD brain as a consequence of increased Aβ load include neuroinflammation and the disruption of the blood-brain barrier (BBB), both of which contribute to the progression of the disease (Soto-Rojas et al., 2015). For example, the abnormal accumulation and spread of Aβ can lead to localized inflammation involving reactive astrocytes with increased glial fibrillary acidic protein (GFAP) expression (Kamphuis et al., 2012), as well as the activation of the microglia that surround Aβ plaques early in the disease (Navarro et al., 2018). In response to high Aβ load and as part of the initiation of the inflammatory process, both astrocytes and microglia likely up-regulate their expression of a surface receptor for the monocyte chemotactic protein-1 (MCP-1), a β-chemokine involved in inflammation that regulates infiltration/migration of macrophages and microglia (Conductier et al., 2010). It has been recently shown that both the severity of AD (Lee et al., 2018b) and the associated memory deficits (Bettcher et al., 2019) correlate with increased plasma levels of MCP-1 in affected humans. Despite evidence supporting microgliosis as a direct response to Aβ load in the AD brain, and/or an indirect process underlying neuronal death (Marín-Teva et al., 2011), the precise role of microglia in the progression of the disease and response to Aβ load has not been fully elucidated. Interferon gamma-induced protein 10 (IP-10) is a pro-inflammatory chemokine that plays a key role in the inflammatory process and is highly expressed in astrocytes in the AD brain (Xia et al., 2000). Furthermore, increasing severity of AD is associated with increased levels of IP-10

(Leung et al., 2013). Aβ load also correlates with the level of astrocytic GFAP expression in 3xTg-AD mice and AD patients (Wyssenbach et al., 2016).

There is increasing evidence to suggest that the BBB is affected by Aβ deposition, which might contribute to its leakage and dysfunction (Erickson and Banks, 2013). The basic functional unit of the BBB is the neurovascular unit (NVU). In capillaries, this consists of endothelial cells connected by tight junctions, pericytes, astrocyte end-feets and extracellular matrix components of the basement membrane (Muoio et al., 2014). Most components of the BBB have been found to contribute to vascular dysfunction in AD (Govindpani et al., 2019, 2020).

A triggering event of AD pathology might be the accumulation of Aβ in the vasculature, leading to a vicious cycle of Aβ aggregation and BBB dysfunction (Govindpani et al., 2020). In this regard, the leakage of fibrinogen, a protein excluded from the brain by the BBB, has been implicated in AD vascular pathology. The fibrinogen-Aβ interaction causes aggregation of fibrinogen and significantly increased BBB permeability through the down-regulation of endothelial tight junction proteins (Cortes-Canteli et al., 2012). Aβ deposition in the vasculature also affects endothelial cell function in the NVU. For instance, endothelial cell adhesion molecules PECAM-1 and ICAM-1 (also known as CD31 and CD54, respectively) play a role in regulating interactions between leukocytes and the endothelium and are involved in the AD pathology through their contribution to the inflammatory process within blood vessels (Wennström and Nielsen, 2012). In the same way, the up-regulation of α-SMA, which plays a role in the contraction of the vessels, might be a compensatory mechanism in late-stage of the AD pathology in response to early vascular disruption in the BBB (Hutter-Schmid and Humpel, 2016).

NFT load has also been found to correlate with the severity of AD (Arriagada et al., 1992). The pathological effect of p-tau in AD may be due to the loss of function of normal tau together with the toxic gain of function of p-tau, which ultimately leads to impaired axonal transport and compromises cell function and homeostasis (Pritchard et al., 2011; Kruger and Mandelkow, 2015; Huber et al., 2017). Neuroinflammation (Lee et al., 2008), compromised BBB function (Nelson et al., 2016) and p-tau accumulation (Huber et al., 2017) are inferred to be the main pathological mechanisms underlying cognitive impairment in AD (Zempel and Mandelkow, 2014; van de Haar et al., 2016; Bettcher et al., 2019). These mechanisms likely promote extensive degeneration of excitatory pathways in brain areas such as the cerebral cortex and hippocampus.

Excitatory N-methyl-D-aspartate receptors are known to mediate $A\beta_{1-42}$-induced excitotoxicity during AD (Liu et al., 2008). Nevertheless, inhibitory pathway disruptions are also well identified in the AD brain (Rissman and Mobley, 2011; Limon et al., 2012; Fuhrer et al., 2017; Govindpani et al., 2017; Kwakowsky et al., 2018). It has been shown that $A\beta_{1-42}$ can increase ambient γ-aminobutyric acid (GABA) concentrations (Kwakowsky et al., 2020; Vinnakota et al., 2020). Recent evidence postulates that this increased ambient GABA level might activate extrasynaptic $GABA_A$ receptors ($GABA_A$Rs) in the hippocampus leading to a chronic depolarizing block through increased tonic inhibition in this area. This results in neural dystrophy and contributes to cognitive decline (Marczynski, 1998; Calvo-Flores Guzmán et al., 2020; Yeung et al., 2020b).

Despite the extensive research in this area, both utilizing *in vitro* and *in vivo* transgenic animal models as well as AD patients, both the definition and the understanding of the disease pathophysiology are far from precise (Govindpani et al., 2017, 2019; Boche and Nicoll, 2020; Harris et al., 2020). Consequently there is a need for a better understanding of the mechanisms underlying Aβ-induced molecular, cellular, and behavioral changes. Some AD rodent models injected with different types of Aβ fragments intraventricularly, or to specific brain regions, have been used to model the disease (Cetin et al., 2013; Faucher et al., 2016; Kwakowsky et al., 2016; Nicole et al., 2016; Schmid et al., 2017). However, it has been shown that the $A\beta_{1-42}$ peptide introduced to neurons *in vitro* and *in vivo* is considerably more neurotoxic than that generated in the AD brain (Klein et al., 1999). This may be because it contains misfolded $A\beta_{1-42}$ and thereby already has enhanced aggregation (Hillen, 2019).

The goal of this study is to elucidate the spatiotemporal progression of $A\beta_{1-42}$-induced pathology and its connection to the resulting synergies of the molecular and cellular changes in p-tau, GFAP, IBA-1, IP-10, MCP-1, ICAM-1, αSMA, CD31, and fibrinogen in the hippocampus, and the resulting behavioral deficits. We have examined the local layer-specific changes of p-tau, and these neuroinflammatory and vascular markers in the CA1 region of the mouse hippocampus using immunohistochemistry and have shown they lead to severe impairment of long-term spatial memory.

MATERIALS AND METHODS

Animals and Brain Tissue Preparation

All experiments were approved and performed following the regulations of the University of Otago and the University of Auckland. All mice were bred and housed at the Hercus Taieri Resource Unit, the University of Otago and Vernon Jansen Unit, University of Auckland, under 12-h reverse light-cycle conditions (lights on at 8 PM), with *ad libitum* access to food and water. All experiments were conducted following the National Animal Ethics Advisory Committee guidelines and with the approval of the institutional animal ethics committee of the University of Otago and the University of Auckland. All experiments were performed on old (18 months; immunohistochemistry, n = 6/group; behavioral testing, n = 12/group) C57BL/6 wild-type male mice.

$A\beta_{1-42}$ Preparation

$A\beta_{1-42}$ is routinely produced as a recombinant protein fused with maltose-binding protein (MBP), with a proteolytic cleavage site for Factor X protease between the two segments based on as used in (Kwakowsky et al., 2020, 2016; Calvo-Flores Guzmán et al., 2020; Yeung et al., 2020a,b). This strategy utilizes the solubilizing character of the MBP, a product of the MalE gene, to ensure the expression of the soluble fusion protein at a high concentration in *Escherichia coli*. After the bacterial expression of

this recombinant fusion protein, the product was purified on an amylose column to which the MBP segment of the protein binds. The affinity selected fusion protein was eluted from the resin with maltose and concentrated by ammonium sulfate precipitation. The carrier MBP was then cleaved off the fusion protein by Factor X protease, and the released $A\beta_{1-42}$ was isolated and further purified by hydrophobic chromatography with 0–50% v/v acetonitrile/0.1% v/v Trifluoroacetic acid (TFA), using fast protein liquid chromatography (FPLC). The fractions containing pure $A\beta_{1-42}$ were detected immunologically with an antibody against residues 17–24 of $A\beta_{1-42}$ and lyophilized to remove the solvent. Mass spectrometry was used to confirm the expected molecular ion for the desired product. The concentration of the protein fragment has been determined by bicinchoninic acid assay at 60°C for 30 min. Before intra-hippocampal injection of this product, we diluted the prepared monomer in artificial cerebrospinal fluid [ACSF: 147 mM Na^+, 3.5 mM K^+, 2 mM Ca^{2+}, 1 mM Mg^{2+} (pH 7.3)] and "aged" the solution at 37°C for 48 h to facilitate the formation of soluble aggregates, which was confirmed by SDS/PAGE and by non-dissociating PAGE (Yeung et al., 2020a). The optimal incubation time required to produce the highly toxic oligomers is 48–120 h depending on the preparation (Kwakowsky et al., 2016; Calvo-Flores Guzmán et al., 2020; Yeung et al., 2020a).

$A\beta_{1-42}$ Stereotaxic Injection

Mice were anesthetized by subcutaneous injection of 75 mg/kg ketamine and 1 mg/kg domitor. Bilateral coordinates for stereotaxic $A\beta_{1-42}$ injection at three depths (antero-posterior, −2.0 mm; medio-lateral, ±1.3 mm; dorso-ventral, −1.8, 2.0, and 2.2 mm from the dura) within the CA1 region of the hippocampus were determined relative to the bregma according to the Paxinos and Franklin's mouse brain atlas (Yeung et al., 2020a,b). Stereotaxic bilateral administration of 1 μl of 20 μM neurotoxic $A\beta_{1-42}$ or scrambled $A\beta_{1-42}$ ($scrA\beta_{1-42}$, AS-25382, AnaSpec) or artificial cerebrospinal fluid (ACSF, used as a vehicle) into the CA1 region was performed at a rate of 0.1 μl/min. The mice in this study were categorized into four groups: naïve control (NC), ACSF, $scrA\beta_{1-42}$, and $A\beta_{1-42}$ injected groups. Naïve control animals did not undergo any surgical procedures.

Behavioral Testing

Behavioral testing was performed to elucidate the effects of $A\beta_{1-42}$ on the cognitive performance of the mice. Specific behavioral tests were used to target different types of hippocampal-dependent memories: (i) long-term spatial memory with the novel object alteration (NOA), novel object recognition (NOR) test, and the Morris water maze (MWM) tests; and (ii) short-term spatial memory with the Y-maze test (YM), as well as short-term non-spatial memory with the passive avoidance test. The O-maze (OM) test was used as a measurement of the anxiety levels of the mice. All behavioral tests were started at 9 am, and analysis was performed using the tracking image analyzer system EthoVision XT 9 (Noldus).

Novel Object Alteration Test

The NOA test was performed to evaluate long-term working memory 7–8 days after injection. The test was performed in a square arena that was surrounded by non-transparent plexiglass walls (25 cm × 29 cm × 25 cm). Each mouse was placed in the arena individually and given 10 min to habituate to the environment. Next, two identical objects were introduced in the arena at designated locations, and the mice were given 5 min to interact with and explore the objects. Following this, each mouse was returned to its cage. The following day (24 h later), one of the identical objects was placed in a new location, and the behavior of the mice was recorded over a 5 min testing period. The testing apparatus was cleaned between animals with 5% acetic acid to minimize olfactory cues. The discrimination ratio (DR) for a novel over a familiar object was calculated as follows: time spent near the object at the new position minus the time spent near the object at the old position, divided by time spent near the object at the new position plus the time spent near the object at the old position.

Novel Object Recognition Test

The NOR test to evaluate long-term recognition memory was performed 11 days after injection. in the same arena as the NOA. During the first 10 min session on day 1, the animal was free to explore the arena, and during the second 5 min session, the animal was able to explore two identical objects. On day 2, one of the objects was replaced by a novel, unfamiliar object, and animal behavior was recorded for 5 min.

The amount of time spent to explore the new object is considered as an index of recognition memory. The DR for a novel over a familiar object was calculated as follows: time spent near the new object minus the time spent near the old object, divided by time spent near the new object plus the time spent near the old object.

Y-Maze Test

Spontaneous exploration and responsiveness to novel environments and short-term spatial memory functions were evaluated with the YM test 15 days post-injection. The apparatus used for the YM study was constructed out of plexiglass with the three arms of the maze positioned at a 120° angle relative to each other. Each arm is identical (52 cm × 12.5 cm); however, different spatial cues were placed in each arm. The start arm for each experiment was chosen randomly: each mouse was placed in the YM environment on two occasions that were separated by a 2 min interval. During the first 5 min trial, one of the three arms was randomly blocked. In the second trial, all the arms were opened for exploration; the total amount of time the mouse took to explore each arm was recorded for 3 min. During the inter-trial interval (2 min), the animal was returned to its home cage and the maze was cleaned. The alternation percentage was calculated as the percentage of the ratio of actual to possible alternations. An index of the time spent in the new, previously unexplored arm as opposed to the familiar explored arm was used to assess any behavioral differences between each group and was calculated as follows: time spent in the new arm minus

time spent in the old arm, divided by time spent in the new arm plus time spent in the old arm.

Morris Water Maze Test

The MWM, a reliable test of spatial memory and hippocampal-dependent learning, was performed at 20 days post-injection (D'Hooge and De Deyn, 2001). The MWM apparatus comprised a circular black tank (diameter, 130 cm; height, 130 cm) filled with tap water and powdered non-fat milk that was added to the tank before the experiment. A constant temperature of 20°C was maintained during the test. A circular escape platform of ∼10 cm diameter and several navigation cues were used to provide spatial orientation for the mice. The starting position of every mouse was assigned randomly. The location of the hidden platform was kept constant (except on the last day of the experiment). If the mouse did not find the hidden platform within 60 s, the animal was guided to the platform for 10 s before being returned to the cage. Spatial learning was tested across four repeat trials over the following 4 days. Between trials, mice were dried with a towel and placed in their cages, located over heating blankets. On the fifth day in each trial, the escape platform was removed, and the time taken to reach the platform quadrant, time spent in the platform quadrant, and distance traveled to reach the platform for each animal were assessed.

Passive Avoidance Test

The passive avoidance test was performed 27 days post-injection. This associative learning task was conducted in a two-compartment box made of one bright compartment and one dark compartment (16 cm × 18 cm). During habituation, the mouse was placed in the bright compartment, and the mouse gained access to the dark compartment. When the mouse entered the dark compartment the door was closed, and the mouse was briefly administered a 0.3-mA electric shock on the foot for 2 s as an aversive stimulus. After 30 s the animal was returned to its home cage. Three hours later, the animal was returned to the bright compartment with the sliding door open. The animal now had the option to avoid or enter the dark compartment. The latency period before the mouse entered the dark compartment was measured.

O-Maze Test

The OM test was performed at 17 days post-injection to assess anxiety-like behaviors. The OM apparatus consisted of a circular maze (40 cm diameter) with two protected (closed) arms, where the mice usually feel safer, and two unprotected (open) arms. Each mouse was randomly placed in one of the closed arms and the behavior was recorded for 5 min. The total time spent by each mouse in the closed and protected arms was measured. Anxiety-like behavior was estimated based on the total time spent in the closed arms of the apparatus, indicating the amount of time spent avoiding the new environment.

Western Blotting

The specificity of the antibodies used in this study had either been tested and reported previously (Yang et al., 2014; Llorian et al., 2016; Wang et al., 2016) or was examined using Western blotting (**Figure 1I**; using a method published previously; Palpagama et al., 2019a,b; Pandya et al., 2019). Mice were euthanized by cervical dislocation and the brains rapidly removed. The brain was cut in half separating the hemispheres on ice; the hippocampus was dissected from each hemisphere of the brain, freshly snap-frozen on dry ice, and stored at −80°C. Tissue was homogenized using a lysis buffer: 4% SDS, 50 mM Tris-HCL, 2 mM EDTA, pH 6.8 supplemented with 0.1% protease inhibitor cocktail (Sigma-Aldrich Co., Saint Louis, MO, USA: P8340) and with 1 mM phenylmethylsulfonyl fluoride (PMSF; Sigma–Aldrich Co., Saint Louis, MO, USA: P7626). A mixture of tissue and lysis buffer was then transferred to centrifuge tubes containing 0.5 mm glass beads. Tissue was homogenized using a Bullet Blender Tissue Homogeniser (Next Advance, Inc., Troy, NY, USA) at speed 8 for 4 min. Samples were then left on the ice to incubate for 1 h and centrifuged at 10,621 *g* for 10 min at 4°C. The supernatant was collected and stored at −20°C. Protein concentrations were determined using a detergent-compatible protein assay (DC Protein assay, 500-0116, Bio-Rad, Hercules, CA, USA), following the manufacturer's instructions. Twenty μg of each protein extract was run on a gradient-polyacrylamide electrophoresis gel (NU PAGE 4–12% BT 1.5, Life Technologies, CA, USA) at 200 V for 45 min using a Thermo Fisher Mini Gel Tank and transferred onto nitrocellulose membranes using the XCell Blot Module (Invitrogen, Waverley, VIC, Australia) at 30 V for 90 min. Membranes were washed in Tris-HCl buffered saline (TBS; pH 7.6) with 0.1% Tween (TBST) and blocked for 30 min at room temperature (RT) with Odyssey blocking buffer (LI-COR Biosciences, USA). The membranes were incubated with primary antibodies (**Table 1**) overnight at 4°C in TBST with 4% BSA (BSA-TBST). The following day, after 3 × 10 min washes in TBST, membranes were incubated at RT for 1 h with an appropriate IRDye (1:10,000, goat anti-rabbit IRDye 680RD, 926-68071, RRID:AB_10956166; goat anti-mouse IRDye 800CW, 926-32210, RRID:AB_621842; donkey anti-goat IRDye 800CW, 926-32214, RRID:AB_621846; LI-COR Biosciences, Lincoln, NE, USA) secondary antibody diluted in 4% BSA-TBST. Detection of immunoreactive bands was performed using the Odyssey Infrared Imaging System (LI-COR Biosciences, USA).

Free-Floating Fluorescence Immunohistochemistry

Mice were deeply anesthetized with 75 mg/kg ketamine and 1 mg/kg domitor and perfused transcardially with 20 ml of ice-cold 4% paraformaldehyde in phosphate buffer (pH 7.6). Brains were removed and postfixed in 4% paraformaldehyde solution for 2 h at RT and then incubated in 30% sucrose in TBS (pH 7.6; 0.05 M Tris-HCl, 0.15 M NaCl) overnight at 4°C. Hippocampal coronal sections (30 μm) were cut on a freezing microtome (Microm International GmbH, Walldorf, Germany) and collected in TBS.

Free-floating fluorescent immunohistochemistry was performed using the method described by Kwakowsky et al. (2016). Briefly, hippocampal sections were washed 3 × 10 min with TBS and incubated in 0.05 M TBS/0.3% Triton/0.25% BSA (TTB)/1% goat serum for 1 h at RT. Sections were then incubated with primary antibodies (**Table 1**) diluted in TTB for 72 h at

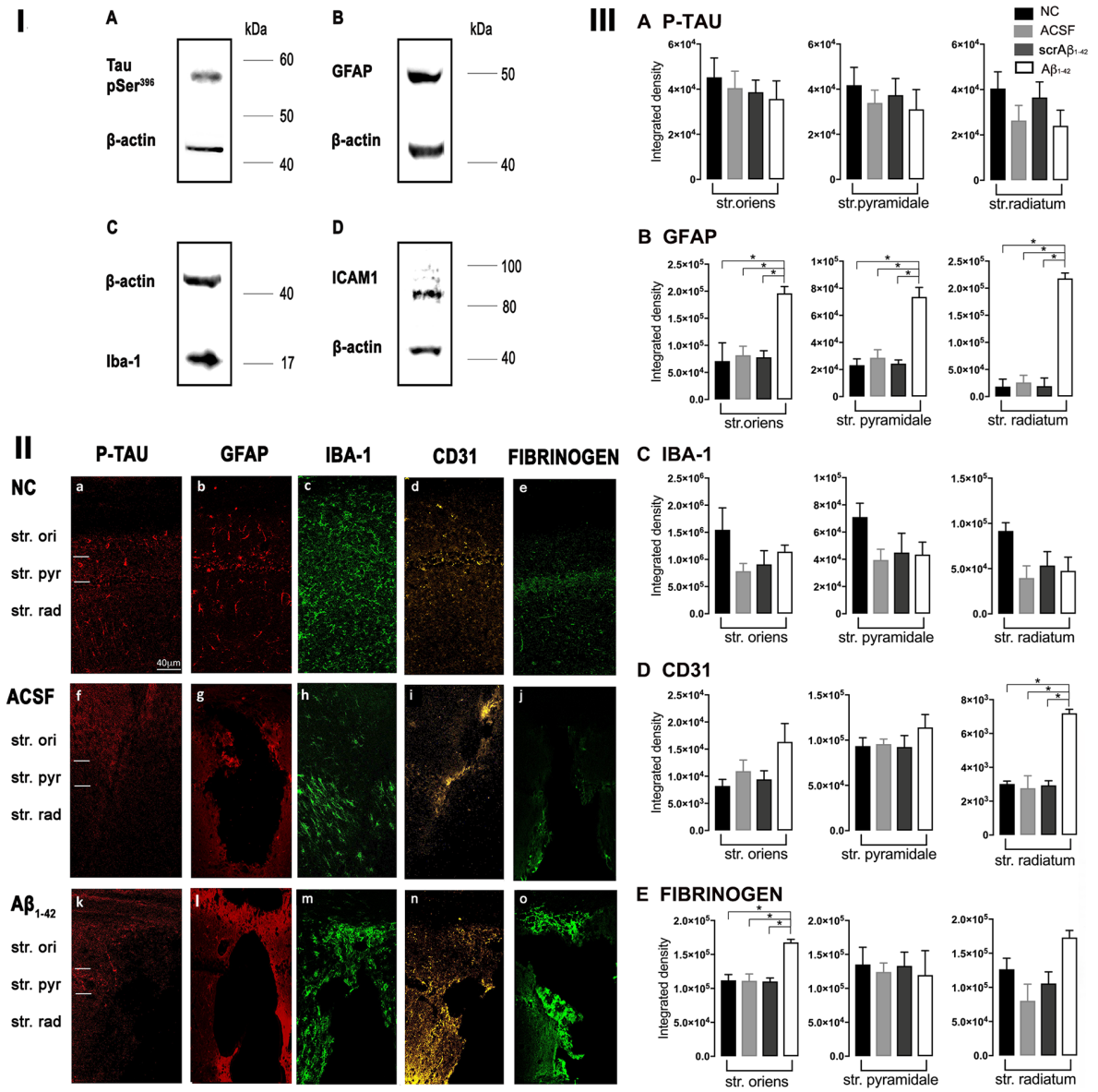

FIGURE 1 | Panel I: Western blot against mouse brain protein homogenates probed with p-tau **(A)**, glial fibrillary acidic protein (GFAP; **B**), Iba-1 **(C)**, and ICAM-1 **(D)**. Observed band sizes: p-tau ∼58 kDA, GFAP ∼50 kDA, Iba-1 ∼17 kDA and ICAM-1 ∼85 kDA. **Panel II:** Representative images showing immunolabeling of p-tau, GFAP, Iba-1, CD31, and fibrinogen at the injection site, 3 days post-injection in NC **(a–e)**, ACSF- **(f–j)**, and $A\beta_{1-42}$-injected **(k–o)** mice. Scale bar (40 μm). **Panel III:** Graphs showing quantification at the injection site in the CA1 hippocampal region of p-tau, GFAP, Iba-1, CD31, and fibrinogen immunolabeling density, 3 days post-injection in NC, ACSF-, $scrA\beta_{1-42}$- and $A\beta_{1-42}$-injected mice. Data expressed as mean ± SEM (Kruskal–Wallis test; $^*p < 0.05$, $n = 3–5$).

4°C on two hippocampal sections from each group. Following 3 × 10 min washes in TBS, sections were incubated in secondary antibodies, goat anti-rabbit Alexa Fluor 647 (1:500, A21245, RRID:AB_141775; Invitrogen, Carlsbad, CA, USA), goat anti-mouse Alexa Fluor 488 (1:500, A11029, RRID: AB_138404; Invitrogen), goat anti-mouse Alexa Fluor 647 (1:500, A21236, RRID:AB_141725; Invitrogen), goat anti-rabbit Alexa Fluor 488 (1:500, A11034, RRID:AB_2576217; Invitrogen), donkey anti-goat Alexa Fluor 647 (1:500, A21447, RRID:AB_141844; Invitrogen) and donkey anti-rabbit Alexa Fluor 488 (1:500, A21206, RRID:AB_141708; Invitrogen) diluted in TTB for 2 h at RT. Finally, the sections were incubated in Hoechst nuclear counterstain (1/10,000 in TTB) for 15 min at RT. Stained sections were examined under a Zeiss LSM 710 confocal laser-scanning microscope (Carl Zeiss, Jena, Germany). The layer-specific labeling of each marker within the CA1 region of the hippocampus was locally analyzed at two specific sites (injection site or needle track, 0–50 μm from the needle track, and adjacent to injection site, 50–500 μm from the needle track) using ImageJ software (U. S. National Institutes of

TABLE 1 | Primary antibodies used in this study.

Antigen	Immunogen	Source, host species, catalog number	Dilution for WB	Dilution for IHC
Anti- Tau pSer396	MAPT(human) mapping to 17q21.31; Mapt(mouse) mapping to 11 E1	Santa Cruz, polyclonal rabbit, sc-101815	1/200	1/100
GFAP cocktail	Equal concentrations of all three monoclonal antibodies (4A11, 1B4, 2E1) that specifically recognize GFAP	BD Biosciences, monoclonal mouse, 556330	1/10,000	1/5,000
Iba-1	A synthetic peptide corresponding to human Iba-1 amino acid 135–147 (C-terminal)	Abcam, polyclonal goat, ab5076	1/500	1/1,000
IP-10	Highly pure (>98%) recombinant hIP 10	Abcam, polyclonal rabbit, ab9807	-	1/100
MCP-1	A recombinant fragment corresponding to human MCP-1	Abcam, polyclonal rabbit, ab9669	-	1/100
α-SMA	N-terminal synthetic decapeptide of α-SMA coupled to keyhole limpet hemocyanin (KLH)	Dako, monoclonal, mouse, M0851	-	1/10
ICAM-1 (CD54)	ICAM-1 (human) mapping too 19p13.2; ICAM-1 (mouse) mapping to 9A3	Santa Cruz, monoclonal mouse, sc-107	1/50	1/50
Fibrinogen	Fibrinogen isolated from human plasma	Dako, polyclonal rabbit, A0080	-	1/500
PECAM-1 (CD31)	Human extracellular domain 1	Dako, monoclonal mouse, M0823	-	1/50
NeuN	Purified cell nuclei from mouse brain	Millipore, monoclonal mouse, MAB377	-	1/1,000

IHC, immunohistochemistry; WB, Western blotting.

Health, Bethesda, MD, USA). After background subtraction and greyscale threshold determination, density measurements were performed for each marker from a defined area of interest measuring 22,748 μm^2 at the injection site and 152,132 μm^2 in each analyzed layer [stratum (str.) oriens, str. pyramidale, str. radiatum] at a location adjacent to the injection site. Particle count and area coverage measurements were conducted using this protocol on the entire field of view of acquired images. Manual counting was performed to determine the number of primary astrocytic and microglial branches. The percentage area coverage by large particles is an indicator of area coverage by activated cells, set at threshold >150 pixels. The percentage area coverage by small particles is the measure of the area covered by the astrocyte and microglia processes. Cells with activated morphology tend to be larger, with more primary branches and an increased number of smaller processes (Glenn et al., 1992; Wilhelmsson et al., 2006; Boche et al., 2013; Palpagama et al., 2019b). The experimenter was blinded to the experimental groupings to eliminate any bias during the experiment, including during image acquisition and analysis. To assess the extent of pyramidal cell loss in the str. pyramidale of the CA1 region of the hippocampus post-$A\beta_{1-42}$ injection, the number of NeuN-positive pyramidal neurons was counted in a 10,296 μm^2 area of the str. pyramidale of the CA1 region. Sections in which the needle track was detected were used for analysis. Two sections were counted per animal (n = 6 in each group) and the results are presented as the number of NeuN-positive pyramidal neurons in the region of interest. Sections with NeuN labeling were examined under a Zeiss LSM 710 inverted confocal laser-scanning microscope (Carl Zeiss, Jena, Germany).

Statistical Analysis

To examine the differences between groups, a Kruskal–Wallis test was conducted for the data obtained, using Graph-Pad Prism software version 8 (GraphPad software, RRID:SCR_002798) with a p-value of $p \leq 0.05$ considered significant, as the data did not meet the assumptions of parametric tests assessed by the D'Agostino–Pearson omnibus and Brown–Forsythe tests. Correlation analysis was performed using Spearman's test. Adobe Photoshop CC 2017 (Adobe Systems Software) was used to prepare the figures.

RESULTS

To assess cell layer-specific changes in tau pathology, density, and morphological changes in neuroinflammatory (GFAP, IBA-1, IP-10, MCP-1) and vascular markers (ICAM-1, αSMA, CD31, fibrinogen) within the CA1 hippocampal region, free-floating fluorescent immunohistochemistry was performed on tissues from NC, ACSF, scr$A\beta_{1-42}$- and $A\beta_{1-42}$-injected mice. Quantification was performed 3 and 30 days post-$A\beta_{1-42}$ injection at sites adjacent to the injection site, as well as at the injection site itself within the CA1 hippocampal region.

Localized $A\beta_{1-42}$-Induced Up-Regulation of GFAP and CD31 by 3 Days Post-$A\beta_{1-42}$ Injection

At the injection site, $A\beta_{1-42}$-injected mice did not display any significant cell loss in the str. pyramidale of the CA1 region at 3 days post-$A\beta_{1-42}$ injection compared with control mice (Yeung et al., 2020a). Localized inflammatory- and vascular pathology-related changes were found in $A\beta_{1-42}$-injected mice compared with ACSF-, scr$A\beta_{1-42}$-injected and NC mice (**Figure 1**, **panel II**). By contrast, p-tau did not show altered expression at the injection site 3 days post-$A\beta_{1-42}$ injection (**Figures 1IIa,f,k,IIIA**). $A\beta_{1-42}$-injected mice exhibited stronger immunostaining of GFAP, Iba-1, CD31, and fibrinogen (**Figure 1III**), markers in the CA1 region at the injection site in comparison with controls. There was an increased GFAP labeling density in comparison with NC, ACSF- and scr$A\beta_{1-42}$-injected mice within the str. oriens (p = 0.0415 vs. NC; p = 0.0499 vs.

ACSF; $p = 0.0315$ vs. $scrA\beta_{1-42}$), str. pyramidale ($p = 0.041$ vs. NC; $p = 0.0491$ vs. ACSF; $p = 0.032$ vs. $scrA\beta_{1-42}$) and str. radiatum ($p = 0.0416$ vs. NC; $p = 0.0421$ vs. ACSF; $p = 0.417$ vs. $scrA\beta_{1-42}$) of the CA1 region (**Figure 1IIIB**). $A\beta_{1-42}$-injected mice showed an increased area coverage by activated cells ($p = 0.049$ vs. NC; $p = 0.049$ vs. ACSF; $p = 0.0235$ vs. $scrA\beta_{1-42}$), a greater number of astrocytes with reactive morphology ($p = 0.0003$ vs. NC; $p = 0.1838$ vs. ACSF; $p = 0.1554$ vs. $scrA\beta_{1-42}$) with increased number of primary branches ($p < 0.0001$ vs. NC; $p = 0.0499$ vs. ACSF; $p = 0.0398$ vs. $scrA\beta_{1-42}$) and increased area coverage by astrocytic processes ($p = 0.0315$ vs. NC; $p = 0.049$ vs. ACSF; $p = 0.0415$ vs. $scrA\beta_{1-42}$; **Figures 2A–D**).

$A\beta_{1-42}$-injected mice also showed an increase in numbers of reactive and dystrophic microglia, but the Iba-1 staining density did not increase (**Figures 1IIm,IIIC**, **2K**). There was also an increased area coverage by activated cells ($p = 0.021$ vs. NC; $p = 0.9321$ vs. ACSF; $p = 0.99$ vs. $scrA\beta_{1-42}$), a greater number of microglia with reactive morphology ($p = 0.0053$ vs. NC; $p = 0.2170$ vs. ACSF; $p = 0.2170$ vs. $scrA\beta_{1-42}$) with increased number of primary branches ($p = 0.0044$ vs. NC; $p = 0.0399$ vs. ACSF; $p = 0.0399$ vs. $scrA\beta_{1-42}$) but the area covered by microglial processes did not change (**Figures 2I–L**).

$A\beta_{1-42}$-injected mice also showed an increased CD31 labeling density in comparison with NC, ACSF- and $scrA\beta_{1-42}$-injected mice within the str. radiatum ($p = 0.0415$ vs. NC; $p = 0.049$ vs. ACSF; $p = 0.0315$ vs. $scrA\beta_{1-42}$) of the CA1 region (**Figure 1IIID**). Fibrinogen displayed increased labeling in the brain parenchyma at the injection site compared with NC, ACSF- and $scrA\beta_{1-42}$-injected mice with a significant increase detected within the str. oriens ($p = 0.042$ vs. NC; $p = 0.042$ vs. ACSF; $p = 0.042$ vs. $scrA\beta_{1-42}$). A similar trend occurred in the str. radiatum but did not reach significance (**Figures 1Ie,j,o,IIE**).

Adjacent to the injection site, despite changes in the pattern of p-tau distribution between groups (**Figure 3Ia,j,s**), quantification of Tau $pSer^{396}$ did not reveal any significant differences between NC, ACSF-, and $scrA\beta_{1-42}$-injected or $A\beta_{1-42}$-injected mice in any layer of the CA1 region 3 days post-$A\beta_{1-42}$ injection (**Figure 3IIA**). However, astrogliosis was revealed by a significant increase in the GFAP labeling intensity between NC, $scrA\beta_{1-42}$-injected and $A\beta_{1-42}$–injected mice in the str. oriens ($p = 0.0021$ vs. NC; $p = 0.0173$ vs. $scrA\beta_{1-42}$), str. pyramidale ($p = 0.036$ vs. NC; $p = 0.0076$ vs. $scrA\beta_{1-42}$) and str. radiatum ($p = 0.0003$ vs. NC; $p = 0.0071$ vs. $scrA\beta_{1-42}$) of the CA1 region of the hippocampus (**Figures 3Ib,k,t,IIB**). $A\beta_{1-42}$-injected mice also displayed an increased GFAP labeling in comparison with ACSF-injected mice within the str. radiatum ($p = 0.0114$) of the CA1 region (**Figure 3IIB**). $A\beta_{1-42}$-injected mice showed a greater number of astrocytes with a highly reactive morphology indicated by numerous branching, elongated processes and hypertrophic cell bodies (**Figure 3It**). $A\beta_{1-42}$-injected mice showed an increased area coverage by activated cells ($p < 0.0001$ vs. NC; $p = 0.02$ vs. ACSF; $p = 0.0305$ vs. $scrA\beta_{1-42}$), a greater number of astrocytes with reactive morphology ($p < 0.0001$ vs. NC; $p = 0.0410$ vs. ACSF; $p = 0.0142$ vs. $scrA\beta_{1-42}$) with increased number of primary branches ($p < 0.0001$ vs. NC; $p = 0.0499$ vs. ACSF; $p = 0.0398$ vs. $scrA\beta_{1-42}$) and increased area coverage by astrocytic processes ($p < 0.0001$ vs. NC; $p = 0.0312$ vs. ACSF; $p = 0.0077$ vs. $scrA\beta_{1-42}$; **Figures 2E–H**).

Despite $A\beta_{1-42}$-injected mice displaying a greater increase in reactive and dystrophic microglia (**Figure 3Iu**), there were no significant differences in Iba-1 density among the groups at 3 days post-$A\beta_{1-42}$ injection at locations adjacent to the injection site (**Figure 3IIc**). $A\beta_{1-42}$-injected mice displayed an increased area coverage by activated microglia ($p < 0.0001$ vs. NC; $p = 0.0275$ vs. ACSF; $p = 0.016$ vs. $scrA\beta_{1-42}$), a greater number of microglia with reactive morphology ($p < 0.0001$ vs. NC; $p = 0.049$ vs. ACSF; $p = 0.0475$ vs. $scrA\beta_{1-42}$) with increased number of primary branches ($p = 0.0012$ vs. NC; $p = 0.0286$ vs. ACSF; $p = 0.0286$ vs. $scrA\beta_{1-42}$) but the area covered by microglial processes did not change (**Figures 2M–P**). Neither IP-10 nor MCP-1 levels, chemokines involved in inflammation, showed significant differences between the groups at 3 days post-$A\beta_{1-42}$ injection (**Figures 3Id,m,v,e,n,w,IID,E**).

Concerning early vasculature disruption, labeling intensity was not significantly different among the groups in the markers ICAM-1 (**Figures 3If,o,x,IIF**), α-SMA (**Figures 3Ig,p,y,IIG**), or fibrinogen (**Figures 3Ii,r,aa,III**). However, $A\beta_{1-42}$-injected mice showed early signs of vascular disruption with significantly up-regulated levels of the endothelial cell marker CD31 adjacent to the injection site in the str. oriens of the CA1 region of the hippocampus compared with NC ($p = 0.0031$), as well as in the str. radiatum of the CA1 region of the hippocampus compared with NC ($p = 0.0131$), ACSF-injected ($p = 0.0387$) and $scrA\beta_{1-42}$-injected mice ($p = 0.0226$; **Figures 3Ih,q,z,IIH**).

These inflammatory (number of GFAP and IBA-1 positive activated cells) and vascular (CD31 and fibrinogen density) pathology markers showed multiple positive cross-correlations (**Figure 4**). For the data obtained at the injections site, these correlations were not statistically significant due to the limited number of sections available from the same animal to test all these markers (**Figures 4A–F**). However, significant positive correlations were observed for most of these markers adjacent to the injection site. The number of activated GFAP positive cells positively correlated with the number of activated microglia ($r = 0.8704$, $p = 0.0028$) and CD31 integrated density ($r = 0.8857$, $p = 0.0333$; **Figures 3G,H**). The number of IBA-1 positive activated cells also correlated with CD31 integrated density ($r = 0.9429$, $p = 0.0167$; **Figure 4I**).

Localized $A\beta_{1-42}$-Induced Pyramidal Cell Loss and Increase in p-tau, GFAP, Iba-1, CD31, and α-SMA by 30 Days Post-injection

By day 30 post-$A\beta_{1-42}$ injection the mice displayed significant neuronal cell loss in the str. pyramidale of the CA1 region of the hippocampus in comparison with the NC (23 ± 0.6 vs. 34.44 ± 1.02, $p < 0.0001$), ACSF-injected (23 ± 0.6 vs. 31.44 ± 0.75, $p = 0.0412$) and $scrA\beta_{1-42}$-injected mice (23 ± 0.6 vs. 32.38 ± 0.86, $p = 0.0069$; **Figure 5IB**). This 33%, 37% and 39% neuronal cell loss in the str. pyramidale of the CA1 region of the hippocampus in the $A\beta_{1-42}$-injected

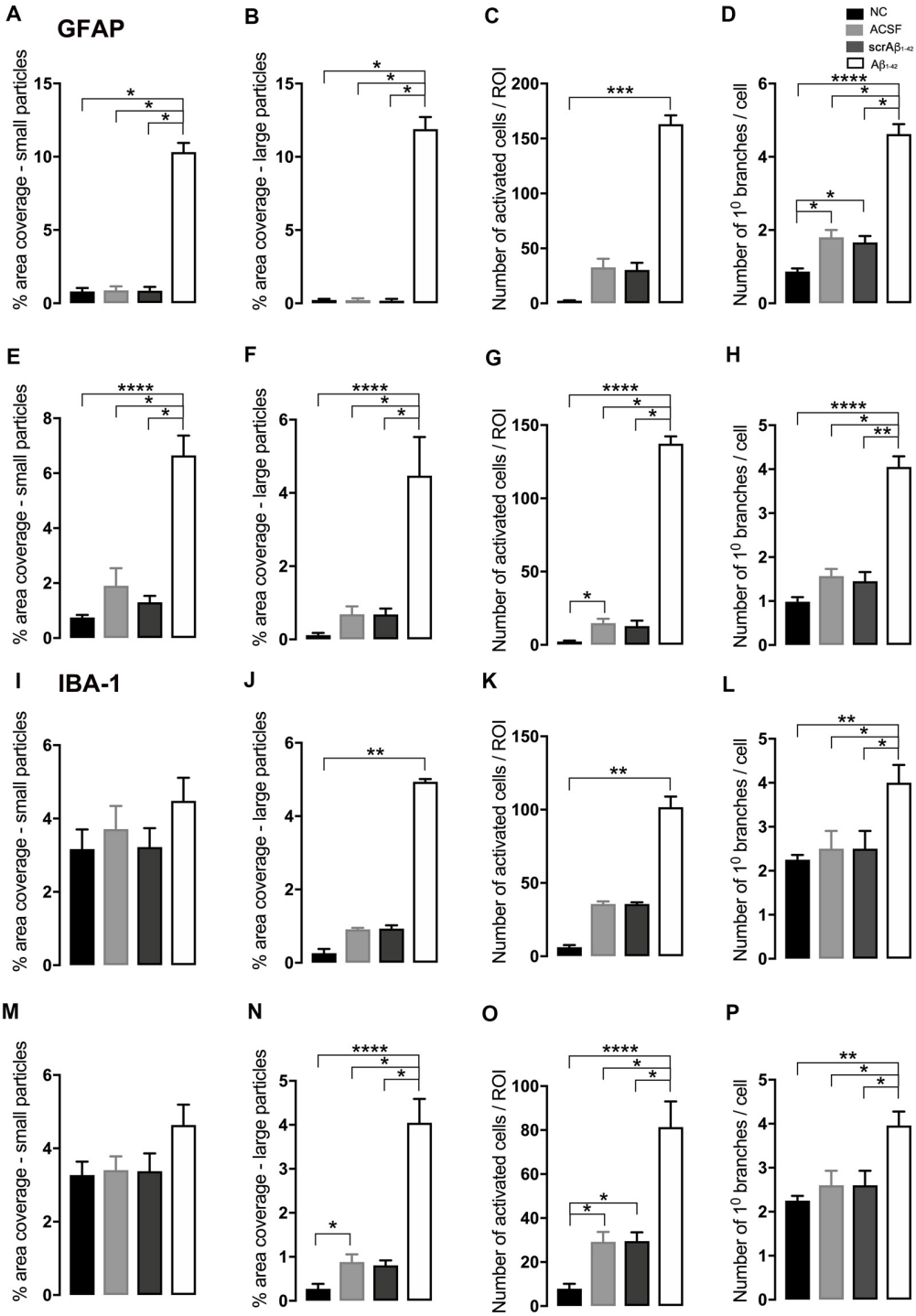

FIGURE 2 | Graphs showing quantification of astrocytic and microglial morphology at the injection site **(A–D,I–L)** and a location adjacent to the injection site **(E–H,M–P)** in the CA1 hippocampal region 3 days post-injection in NC, ACSF-, scrAβ_{1-42}- and Aβ_{1-42}-injected mice. Data expressed as mean ± SEM (Kruskal–Wallis test; *$p < 0.05$; **$p < 0.01$, ***$p < 0.001$, ****$p < 0.0001$, $n = 3$–6).

mice in comparison with the NC mice, ACSF-, and scrAβ_{1-42}-injected controls respectively (**Figure 5IB**) is indicative of Aβ_{1-42}-induced neurotoxicity, as well as the long-lasting impact of a single bilateral intra-hippocampal injection of Aβ_{1-42}. Visualization of NeuN-positive pyramidal cells in the str. pyramidale of the CA1 hippocampal region of Aβ_{1-42}-injected mice demonstrated that apart from the considerable amount of cell loss, the remaining pyramidal cells had an irregular shape

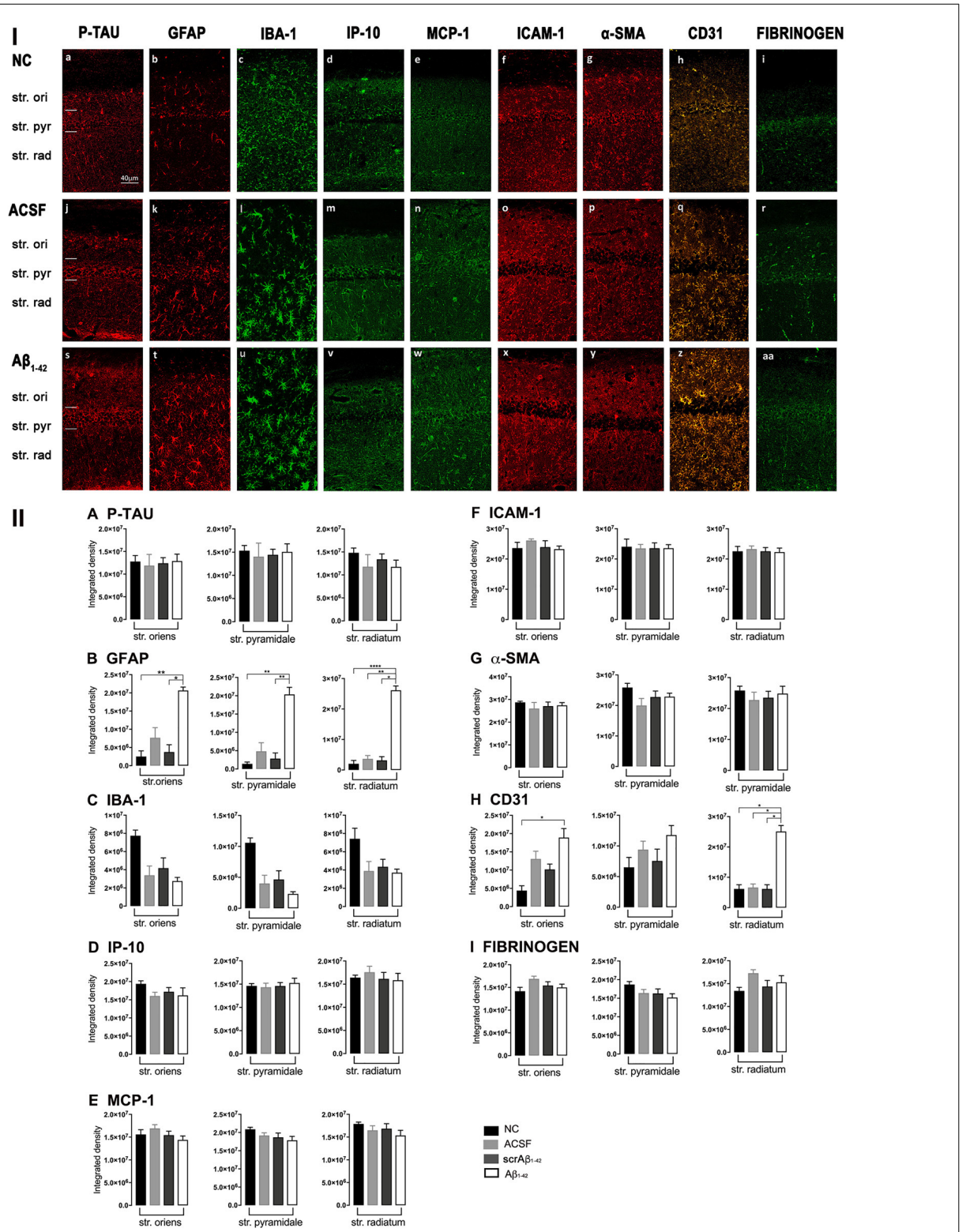

FIGURE 3 | Panel I: Representative images showing immunolabeling of p-tau, GFAP, Iba-1, IP-10, MCP-1, ICAM-1, α-SMA, CD31, and fibrinogen at a location adjacent to the injection site, 3 days after injection in NC **(a–i)**, ACSF- **(j–r)** and $A\beta_{1-42}$-injected **(s–aa)** mice. Scale bar (40 μm). **Panel II:** Graphs showing quantification at a location adjacent to the injection site in the CA1 hippocampal region of p-tau, GFAP, Iba-1, IP-10, MCP-1, ICAM-1, α-SMA, CD31, and fibrinogen **(A–I)** immunolabeling density, 3 days post-injection in NC, ACSF-, $scrA\beta_{1-42}$- and $A\beta_{1-42}$-injected mice. Data expressed as mean ± SEM (Kruskal–Wallis test; $^{*}p < 0.05$; $^{**}p < 0.01$, $^{****}p < 0.0001$, $n = 6$).

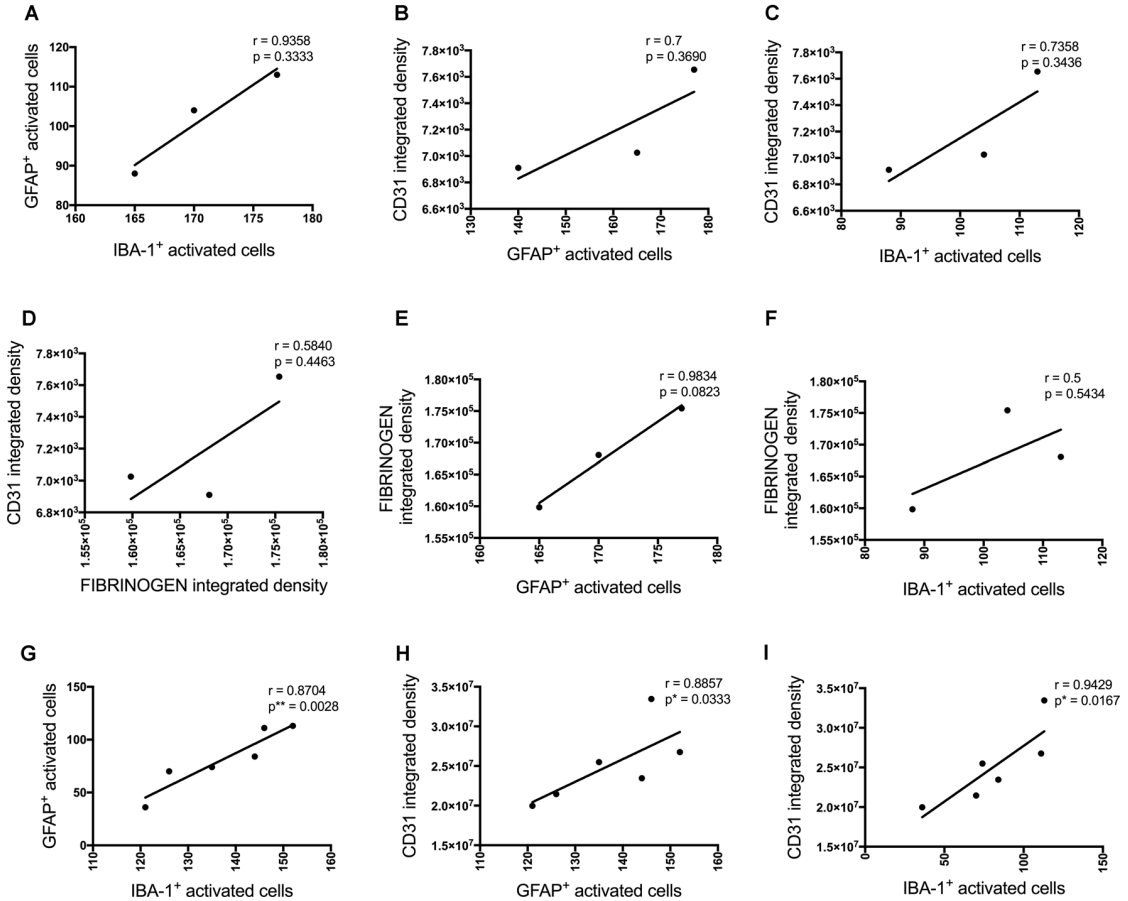

FIGURE 4 | Correlation between the number of activated astrocytes and microglia and vascular markers at the injection site (**A–F**, $n = 3$) and a location adjacent to the injection site (**G–I**, $n = 6$) in the CA1 hippocampal region 3 days post-injection in NC, ACSF-, scrAβ$_{1-42}$- and Aβ$_{1-42}$-injected mice. This relationship is represented by a Spearman's r-value (*$p < 0.05$, **$p < 0.01$).

in Aβ$_{1-42}$-injected mice (**Figure 5IC**). We have also found a significant 12%, 15% and 13% pyramidal cell loss at 7 days after Aβ$_{1-42}$ injection in the CA1 hippocampal region of the mice compared to NC (56 ± 1.2 vs. 64 ± 1.34, $p = 0.0458$), ACSF- (56 ± 1.2 vs. 66 ± 1.59, $p = 0.0164$) and scrAβ$_{1-42}$-injected mice, respectively (**Figure 5IA**).

At the injection site, significant localized tau hyperphosphorylation, inflammation, and vascular changes were found in Aβ$_{1-42}$-injected mice 30 days post-injection compared with ACSF-injected and NC mice (**Figures 5II,III**). This conclusion was derived from localized Aβ$_{1-42}$ injection-induced increase in p-tau, GFAP, and Iba-1 levels and the up-regulation of CD31 at the injection site (**Figure 5IIk–m**). By 30 days after the injection, p-tau immunoreactivity in the str. oriens, str. pyramidale and str. radiatum of the CA1 region of the hippocampus was significantly higher in the Aβ$_{1-42}$-injected mice compared to NC ($p < 0.0001$), ACSF- ($p = 0.0439$; $p = 0.044$; $p = 0.0123$) and scrAβ$_{1-42}$-injected mice ($p = 0.0057$; $p = 0.0058$; $p = 0.0229$; **Figures 5IIa,f,k,IIIA**). Aβ$_{1-42}$-injected mice showed stronger p-tau immunoreactivity within the somatodendritic compartments of neurons in the str. pyramidale and along axonal processes extending from the str. pyramidale compared with control mice (**Figure 5IIa,f,k**).

In addition, astrogliosis was observed at the injection site by 30 days after the Aβ$_{1-42}$ injection, as indicated by the significant increase in GFAP labeling in the str. oriens, str. pyramidale and str. radiatum in the Aβ$_{1-42}$-injected mice in comparison with the NC ($p < 0.0001$), ACSF- ($p = 0.0168$; $p = 0.0439$; $p = 0.0058$) and scrAβ$_{1-42}$-injected mice ($p = 0.0168$; $p = 0.0057$; $p = 0.044$; **Figure 5IIIB**). The ACSF- and scrAβ$_{1-42}$-injected mice also displayed significantly higher GFAP immunoreactivity than the NC mice in the str. oriens ($p = 0.0168$; $p = 0.0168$), str. pyramidale ($p = 0.0057$; $p = 0.0439$) and str. radiatum ($p = 0.044$; $p = 0.0058$; **Figure 5IIIB**). Aβ$_{1-42}$-injected mice showed an increased area coverage by activated cells ($p = 0.0001$ vs. NC; $p = 0.0151$ vs. ACSF; $p = 0.0095$ vs. scrAβ$_{1-42}$), a greater number of astrocytes with reactive morphology ($p = 0.0005$ vs. NC; $p = 0.049$ vs. ACSF; $p = 0.037$ vs. scrAβ$_{1-42}$), increased area coverage by astrocytic processes ($p = 0.0128$ vs. NC; $p = 0.1651$ vs. ACSF; $p = 0.0455$ vs. scrAβ$_{1-42}$) but the number of primary branches did not change (**Figures 6A–D**).

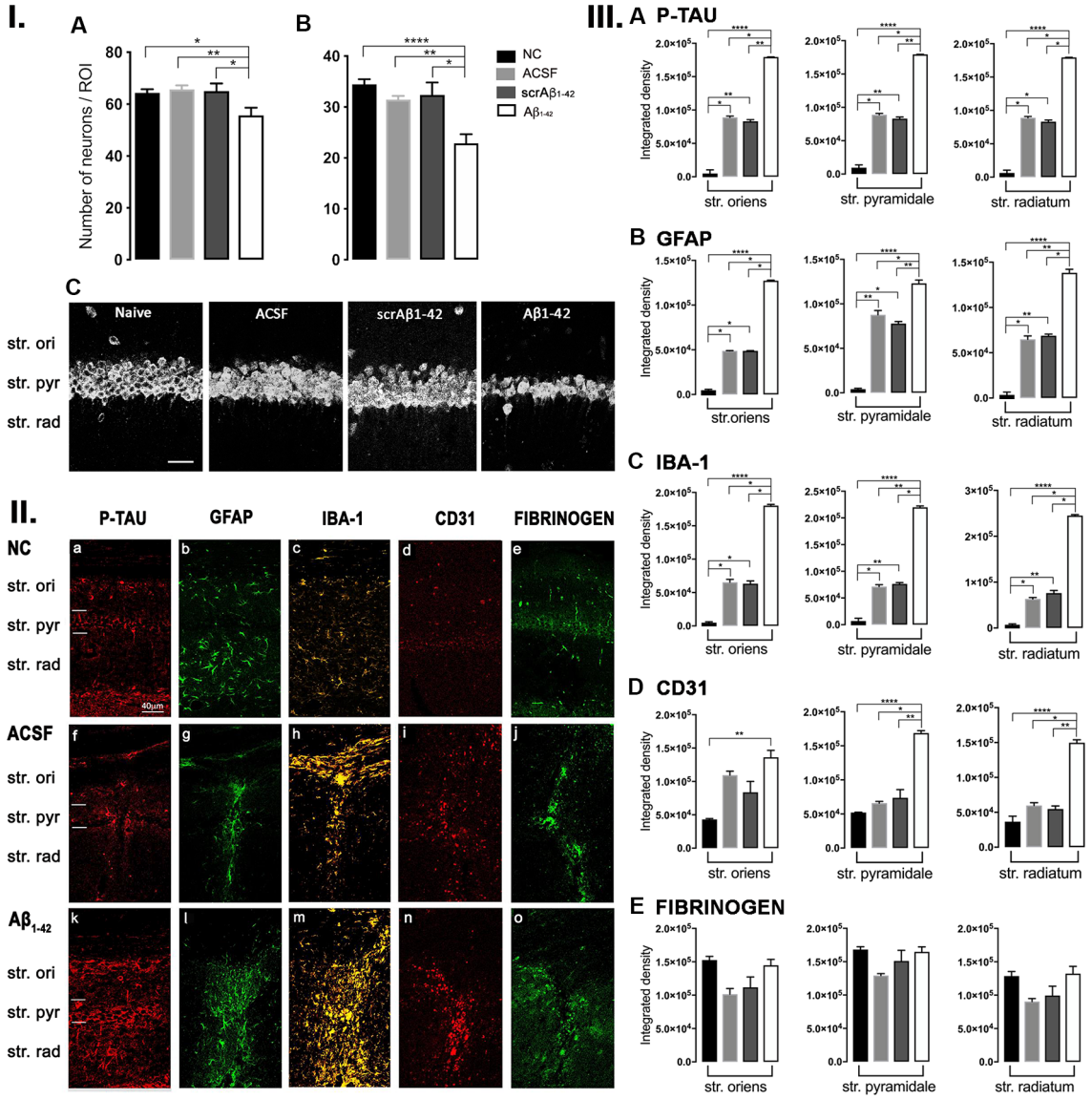

FIGURE 5 | Panel I: Graphs showing the number of NeuN-positive pyramidal cells in the str. pyramidale of the CA1 hippocampal layer in NC, ACSF-, scrAβ_{1-42}- and Aβ_{1-42}-injected mice 7 days post-injection **(A)** and 30 days post-injection **(B)**. Representative images of the CA1 hippocampal subregion at a location adjacent to the injection site showing NeuN-positive pyramidal cells from the str. pyramidale in NC, ACSF-, scrAβ_{1-42}- and Aβ_{1-42}-injected mice 30 days post-injection **(C)**. **Panel II:** Representative images showing immunolabeling of p-tau, GFAP, Iba-1, CD31, and fibrinogen at the injection site 30 days post-injection in NC **(a–e)**, ACSF-injected **(f–j)**, and Aβ_{1-42}-injected **(k–o)** mice. Scale bar (40 μm). **Panel III:** Graphs showing quantification at the injection site in the CA1 hippocampal region of p-tau, GFAP, Iba-1, CD31, and fibrinogen, 30 days post-injection in NC, ACSF-, scrAβ_{1-42}- and Aβ_{1-42}-injected mice. Data expressed as mean ± SEM (Kruskal–Wallis test; $^{*}p < 0.05$; $^{**}p < 0.01$, $^{****}p < 0.0001$, $n = 6$).

Likewise, localized microgliosis, as indicated by the increase in Iba-1 density, in the str. oriens, str. pyramidale and str. radiatum was significantly increased in the Aβ_{1-42}-injected mice compared with the NC ($p < 0.0001$), ACSF- ($p = 0.0229$; $p = 0.0058$; $p = 0.0052$) and scrAβ_{1-42}-injected mice ($p = 0.0124$; $p = 0.044$; $p = 0.0475$; **Figure 5IIIC**). The ACSF- and scrAβ_{1-42}-injected mice also displayed higher Iba-1 levels than the NC mice in the str. oriens ($p = 0.0124$; $p = 0.0229$), str. pyramidale ($p = 0.044$; $p = 0.0058$) and str. radiatum ($p = 0.0475$; 0.0052) of the CA1 region (**Figure 5IIIC**). Aβ_{1-42}-injected mice displayed an increased area coverage by activated microglia ($p < 0.0001$ vs. NC; $p = 0.0269$ vs. ACSF; $p = 0.049$ vs. scrAβ_{1-42}) and a greater number of microglia with reactive morphology ($p < 0.0001$ vs. NC; $p = 0.0151$ vs. ACSF; $p = 0.0261$ vs. scrAβ_{1-42}) but the number of primary branches and the area covered by microglial processes did not change (**Figures 6I–L**).

Localized changes in vascular markers at the injection site were also observed in Aβ_{1-42}-injected mice by 30 days

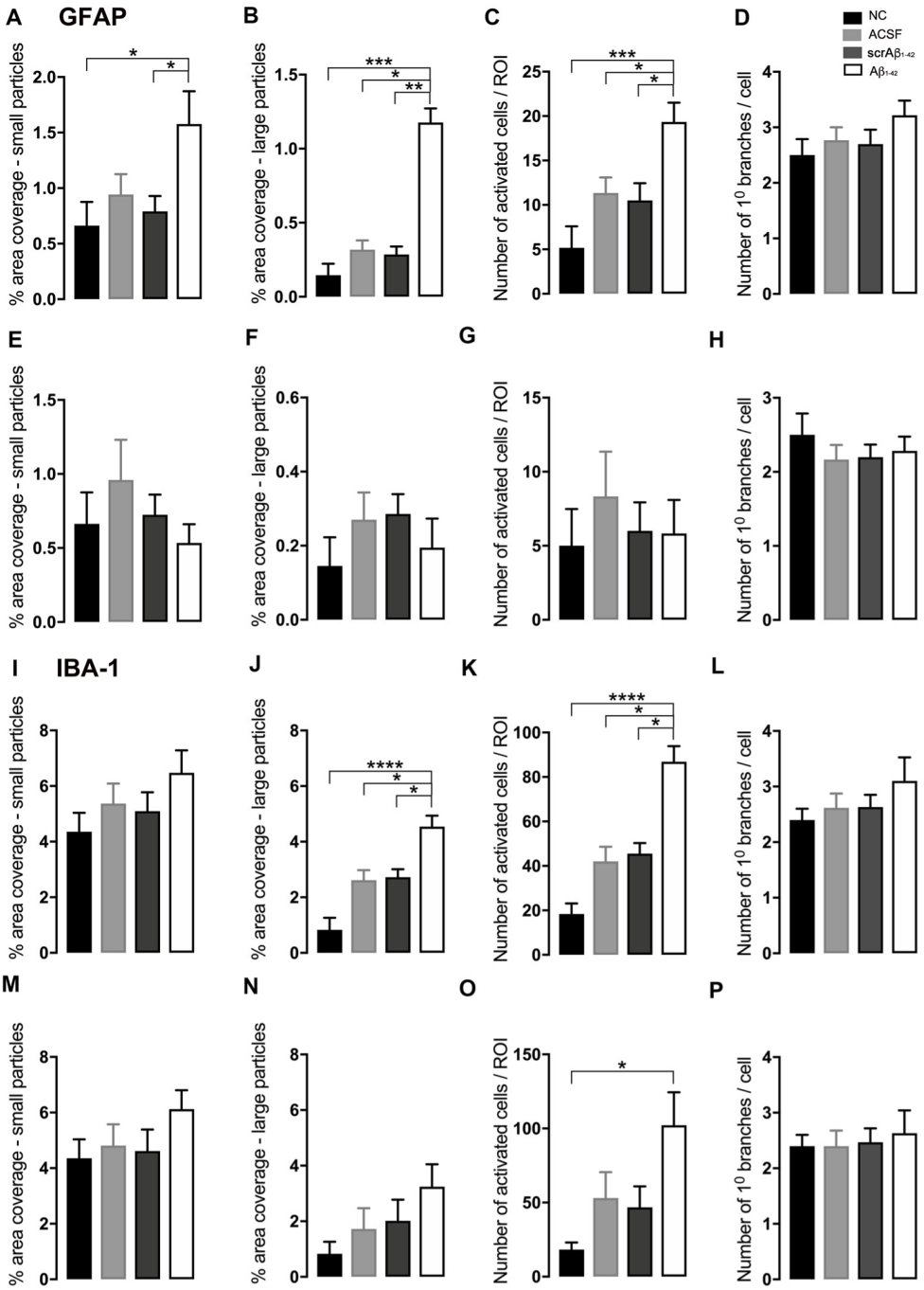

FIGURE 6 | Graphs showing quantification of astrocytic and microglial morphology at the injection site **(A–D,I–L)** and a location adjacent to the injection site **(E–H,M–P)** in the CA1 hippocampal region 30 days post-injection in NC, ACSF-, scrAβ_{1-42}- and Aβ_{1-42}-injected mice. Data expressed as mean ± SEM (Kruskal–Wallis test; *$p < 0.05$, **$p < 0.01$, ***$p < 0.001$, ****$p < 0.0001$, $n = 6$).

after the injection as compared to the controls. CD31 levels were significantly higher in the Aβ_{1-42}-injected mice than in the NC mice in the str. oriens, str. pyramidale, and str. radiatum of the CA1 region of the hippocampus ($p = 0.0002$; $p < 0.0001$; $p < 0.0001$; **Figures 5IIn,IIID**). The Aβ_{1-42}-injected mice also displayed higher CD31 levels than the ACSF- and scrAβ_{1-42}-injected mice in the str. pyramidale ($p = 0.0135$; $p = 0.0025$) and str. radiatum ($p = 0.0162$; $p = 0.0042$) of the CA1 region of the hippocampus (**Figure 5IIID**).

In addition to the vascular changes found at the injection site, 30 days post-injection, there was a significant increase

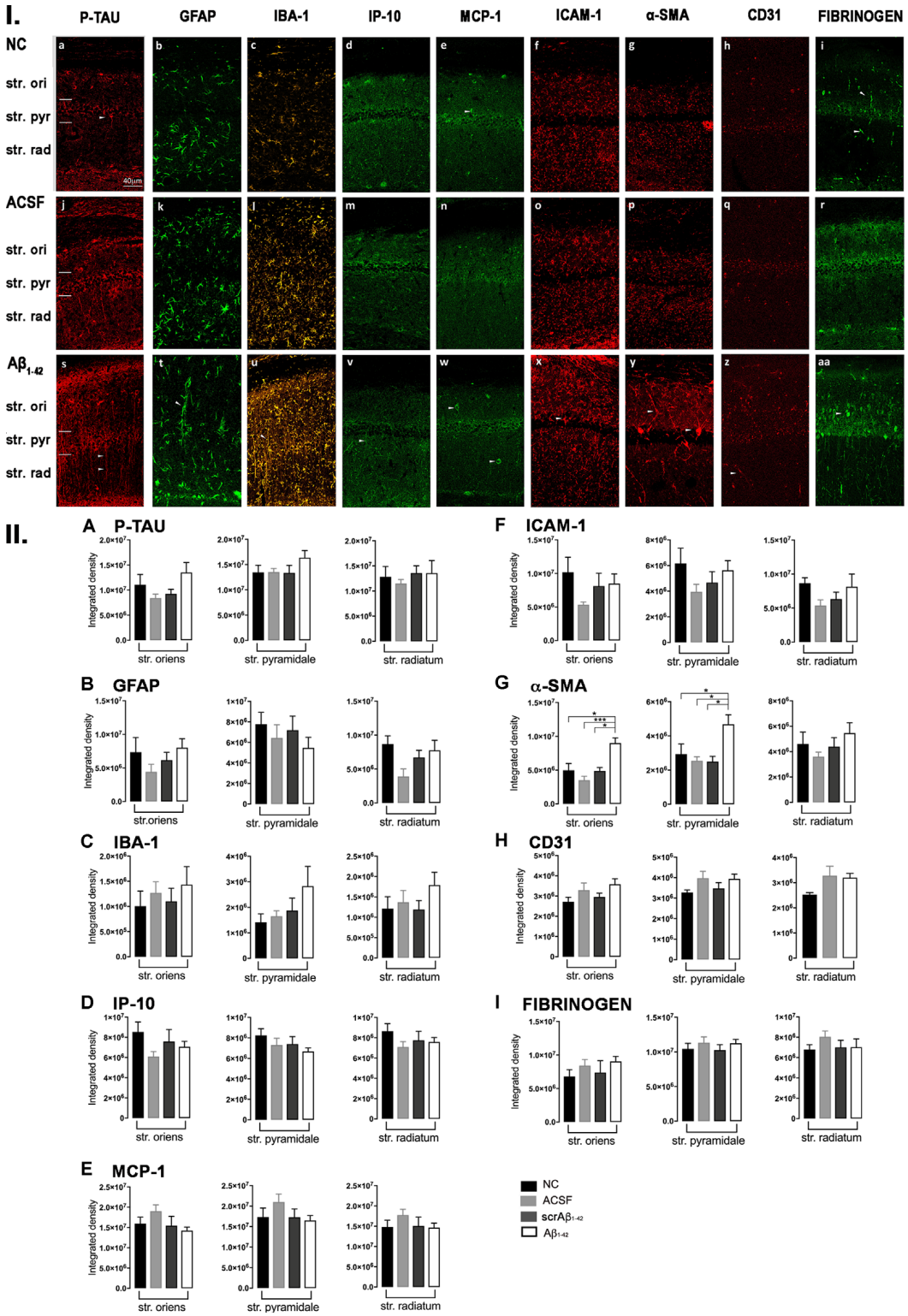

FIGURE 7 | Panel I: Representative images showing immunolabeling of p-tau, GFAP, Iba-1, IP-10, MCP-1, ICAM-1, a-SMA, CD31 and fibrinogen at a location adjacent to the injection site, 30 days post- injection in NC **(a–i)**, ACSF-injected **(j–r)** and $A\beta_{1-42}$-injected **(s–aa)** mice. **Panel II:** Graphs showing quantification at a location adjacent to the injection site in the CA1 hippocampal region of p-tau, GFAP, Iba-1, IP-10, MCP-1, ICAM-1, α-SMA, CD31 and fibrinogen immunolabeling density, 30 days post injection in NC, ACSF-, scrAb1–42- and Ab1–42-injected mice. Data expressed as mean SEM (Kruskall–Wallis test; $^{*}p < 0.05$; $^{***}p < 0.001$, $n = 6$).

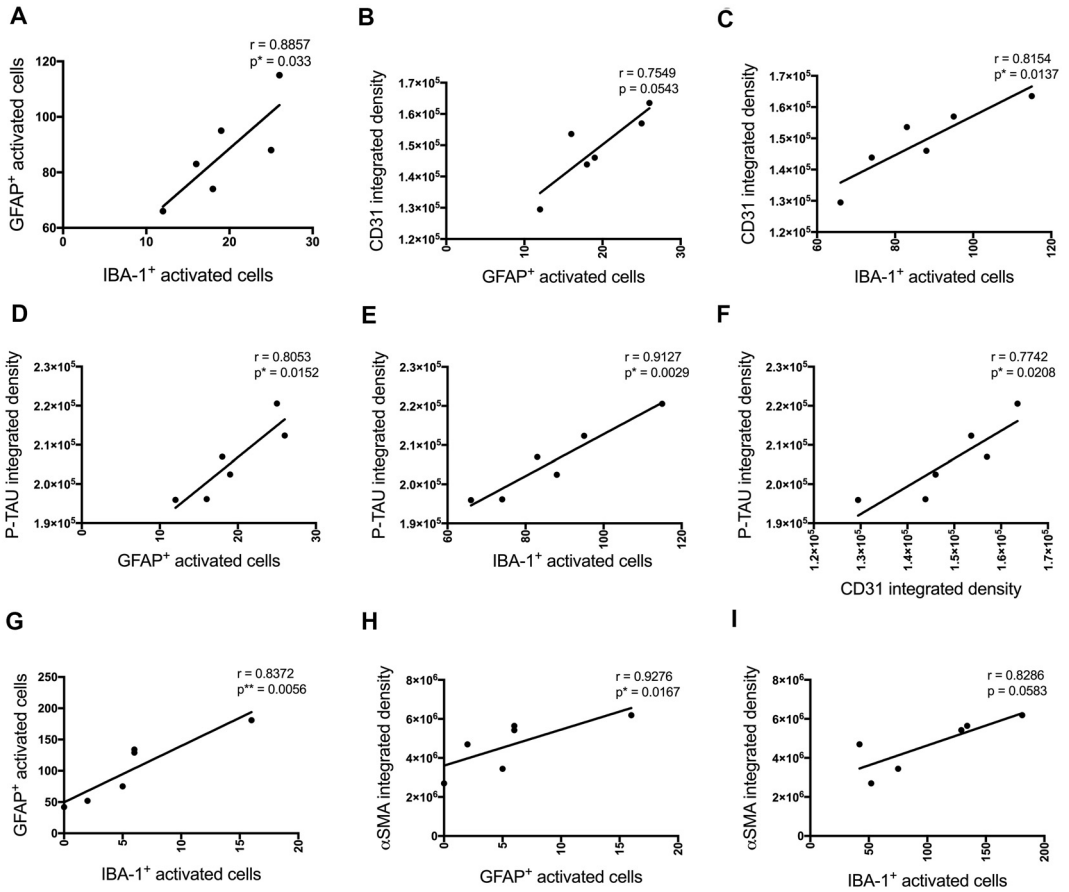

FIGURE 8 | Correlation between the number of activated astrocytes and microglia, p-tau, and vascular markers at the injection site **(A–F)** and at a location adjacent to the injection site **(G–I)** in the CA1 hippocampal region 30 days post-injection in NC, ACSF-, scrAβ_{1-42}- and Aβ_{1-42}-injected mice. This relationship is represented by a Spearman's *r*-value (*$p < 0.05$, **$p < 0.01$, $n = 6$).

in α-SMA density at a location adjacent to the injection site in Aβ_{1-42}-injected mice compared with NC, ACSF and scrAβ_{1-42}-injected mice in the str. oriens ($p = 0.0180$ vs. NC; $p = 0.0008$ vs. ACSF; $p = 0.0143$ vs. scrAβ_{1-42}) and str. pyramidale ($p = 0.0241$; vs. NC; $p = 0.0246$ vs. ACSF; $p = 0.0136$ vs. scrAβ_{1-42}; **Figures 7Iy,IIG**). Although we did not find any other significant Aβ_{1-42}-induced effects at the location adjacent to the injection site for p-tau, Iba-1, IP-10, MCP-1, ICAM-1, CD31, and fibrinogen (**Figures 7I;IIA,D,E,F,H,I**), Aβ_{1-42}-injected mice showed a non-significant trend towards increased p-tau in the str. oriens of the CA1 hippocampal region (**Figure 7Is**). Astrocyte morphology did not differ from controls in Aβ_{1-42}-injected mice (**Figures 6E–H**) but activated microglia numbers were slightly increased compared with NC ($p = 0.0019$), ACSF- ($p = 0.1208$) and scrAβ_{1-42}-injected mice ($p = 0.0864$; **Figures 6M–P**).

P-tau, some inflammatory- (number of GFAP and IBA-1 positive activated cells) and vascular (CD31 and α-SMA density) pathology markers showed multiple positive correlations (**Figure 8**). Significant positive correlations were observed for most of these markers at the injection site and adjacent to the injection site as well. The number of activated GFAP positive cells positively correlates with the number of activated microglia ($r = 0.8857$, $p = 0.033$ injection site; $r = 0.8372$, $p = 0.0056$ adjacent injection site), CD31 ($r = 0.7549$, $p = 0.0543$), p-tau ($r = 0.8053$, $p = 0.0152$) and α-SMA ($r = 0.9276$, $p = 0.0167$ adjacent injection site) integrated density (**Figures 8A,B,D,G,H**). The number of IBA-1 positive activated cells also correlates with CD31 ($r = 0.8154$, $p = 0.0137$) and p-tau ($r = 0.9127$, $p = 0.0029$) integrated density (**Figures 8C,E**).

Aβ1–42-Induced Behavioral and Cognitive Changes

To elucidate the long-lasting effect of Aβ_{1-42} treatment on cognitive function at the 7–30-day time points the NOA, NOR and MWM tests for long-term spatial-memory were performed, as well as the YM test for short-term spatial memory, the passive avoidance test for short-term non-spatial memory, and the OM test as a measurement of the anxiety levels in the mice (**Figures 9A–F**).

According to the results of NOA (**Figure 9A**), the Aβ_{1-42}-injected mice showed significant cognitive deterioration in long-term spatial memory as compared with the NC ($p = 0.0308$),

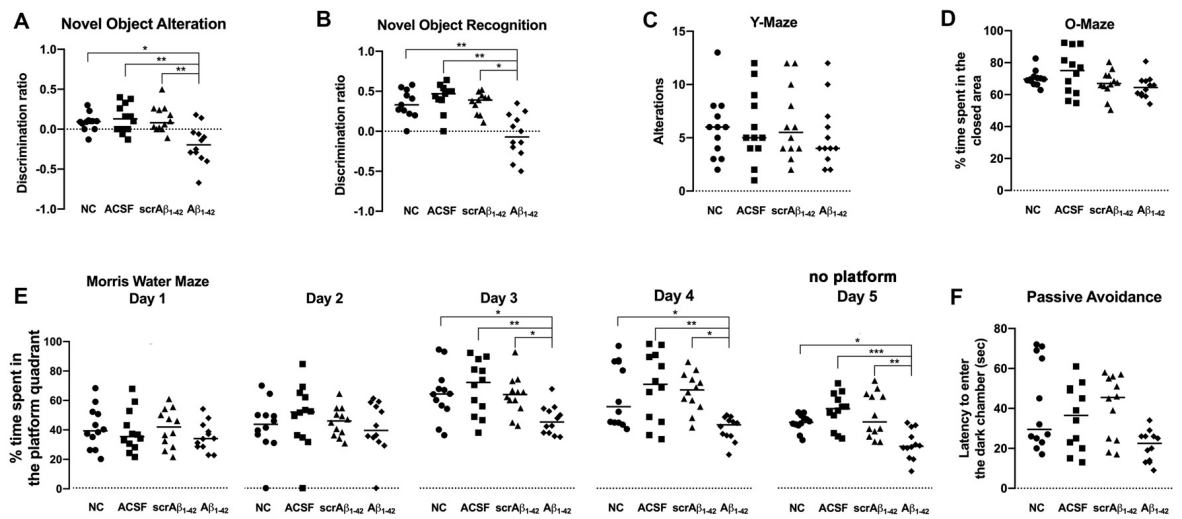

FIGURE 9 | $A\beta_{1-42}$-injected mice showed long-term spatial memory impairment revealed by the novel object alteration (**A**, performed on days 7, 8), novel object recognition (**B**, performed on days 11, 12), and Morris Water Maze (**E**, performed on days 20–24) tests. Short-term spatial memory assessed by the Y maze showed no significant difference in $A\beta_{1-42}$-injected mice compared with controls (**C**, performed on day 15). Non-spatial memory remained unchanged in $A\beta_{1-42}$-injected mice compared with controls (**F**, performed on day 27), and $A\beta_{1-42}$ and/or the injection itself did not produce any anxiogenic effect (**D**, performed on day 17). Scatter plot showing all of the data values used with the median (Kruskal-Wallis test; $^{*}p < 0.05$; $^{**}p < 0.01$, $^{***}p < 0.001$, $n = 12$).

ACSF- ($p = 0.0082$), and $scrA\beta_{1-42}$-injected mice ($p = 0.0089$), with significantly lower DR at 8 days post-injection (**Figure 9A**).

The $A\beta_{1-42}$-injected mice also showed significant cognitive deterioration in long-term spatial memory as compared with the NC ($p = 0.0099$), ACSF- ($p = 0.0003$), and $scrA\beta_{1-42}$-injected mice ($p = 0.0127$) according to the results of the NOR test at 12 days post-injection (**Figure 9B**).

According to the MWM test, the $A\beta_{1-42}$-injected mice also showed significant long-term spatial memory impairment when compared with the NC, ACSF- and $scrA\beta_{1-42}$-injected mice (**Figure 9E**). During day 1 and 2 of the MWM test (20 and 21 days post-injection), the mice from the three groups spent a similar amount of time in the platform quadrant of the maze, but significant differences were found between the NC, ACSF- and $scrA\beta_{1-42}$-injected mice and the $A\beta_{1-42}$-injected mice during day 3 and 4 of the experiment: the $A\beta_{1-42}$-injected mice spent significantly less time in the platform quadrant than the NC ($p = 0.0401$; $p = 0.0498$), ACSF-injected mice ($p = 0.008$; $p = 0.0064$) and the $scrA\beta_{1-42}$ mice ($p = 0.0437$; $p = 0.0129$ for day 3 and 4 respectively). During the fifth and last day of the test, when the platform was removed, the time spent by each group at the "platform quadrant" was also assessed. The $A\beta_{1-42}$-injected mice spent significantly less time in the platform quadrant on day 5, as compared with the NC ($p = 0.0287$), ACSF- ($p = 0.0003$) and $scrA\beta_{1-42}$-injected mice ($p = 0.0072$; **Figure 9E**). Therefore, data from the MWM test show that whereas the control mice showed successful learning from day 3, the $A\beta_{1-42}$-injected mice presented with long-term spatial memory impairment which affected their performance on days 3 and 4, as well as the last day of the test (**Figure 9E**).

According to the findings of the YM test, there was no significant difference in short-term spatial memory between any of the treatment groups 15 days post-injection. This indicates that short-term spatial memory was not affected by $A\beta_{1-42}$ injection. Alternatively, it is also possible that any effect on short-term spatial memory could not be detected by this test. However, although the performance of the mice was similar across all the groups, the $A\beta_{1-42}$-injected mice showed a slightly decreased number of alternations as compared with the NC, ACSF- and $scrA\beta_{1-42}$-injected mice (**Figure 9C**).

The $A\beta_{1-42}$-injected mice showed no significant difference in non-spatial memory performance as compared with the NC ($p = 0.0739$), ACSF- ($p = 0.3766$) and $scrA\beta_{1-42}$-injected mice ($p = 0.0539$) by 28 days post-injection (**Figure 9F**). In phase 3 of the passive avoidance test (post-shock 3 h), similar latency to enter the dark chamber was found in the control and $A\beta_{1-42}$-injected mice (**Figure 9F**).

Since anxiety is likely to influence cognitive performance, the OM test was performed to determine whether the mice from the different treatment groups exhibited anxiety. The $A\beta_{1-42}$-injected mice showed no significant difference in anxiety levels as compared with the NC, ACSF- and $scrA\beta_{1-42}$-injected mice (**Figure 9D**), as mice from all the groups were found to spend a similar amount of time in the closed (protected) arm of the O-maze apparatus. Thus, $A\beta_{1-42}$ and/or the injection itself did not produce any anxiogenic effect (**Figure 9D**).

Cognitive performance of $A\beta_{1-42}$-injected mice after showed a negative correlation with p-tau density (NOA $r = -0.8469$, $p = 0.0238$; NOR $r = -0.8117$, $p = 0.0722$; MWM $r = -0.8286$, $p = 0.0573$; **Figures 10G–I**), the number of activated astrocytes (NOA $r = -0.6571$, $p = 0.175$; NOR $r = -0.8986$, $p = 0.0278$; MWM $r = -0.8857$, $p = 0.0333$; **Figures 10A–C**) and microglia (NOA $r = -0.9429$, $p = 0.0167$; NOR $r = -0.8986$,

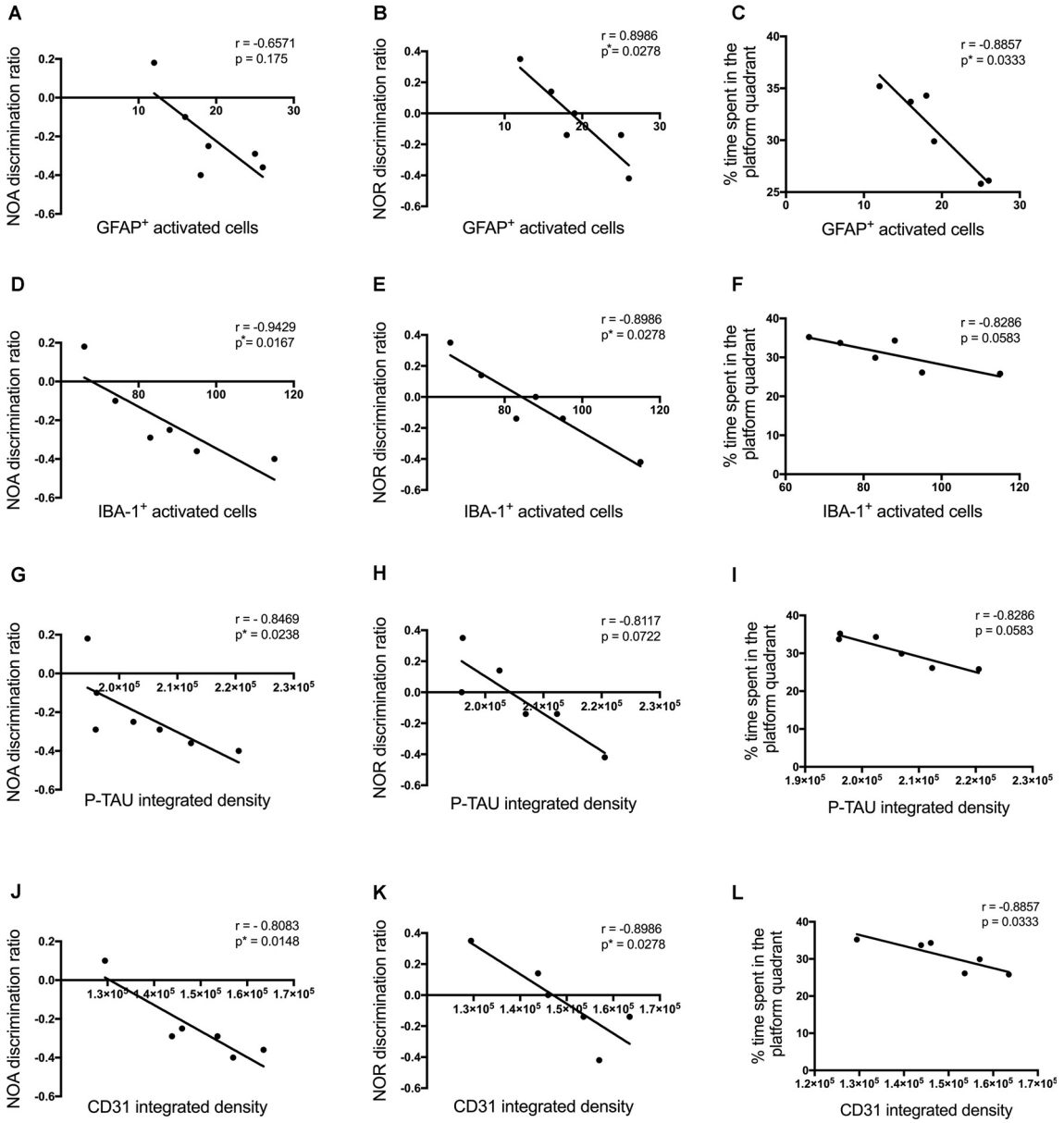

FIGURE 10 | Correlation between the number of activated astrocytes and microglia **(A–F)**, p-tau **(G–I)**, CD31 **(J–L)**at the injection site in the CA1 hippocampal region, and behavioral scores 30 days post-injection in NC, ACSF-, scrAβ$_{1–42}$- and Aβ$_{1–42}$-injected mice. This relationship is represented by a Spearman's *r*-value (*$p < 0.05$, $n = 6$).

$p = 0.0278$; MWM $r = -0.8286$, $p = 0.0583$; **Figures 10D–F**) and CD31 density (NOA $r = -0.8083$, $p = 0.0148$; NOR $r = -0.8986$, $p = 0.0278$; MWM $r = -0.8857$, $p = 0.0333$; **Figures 10J–L**), but no significant correlations were observed with other inflammatory, vascular markers or neuronal loss.

DISCUSSION

The present study is an in-depth holistic molecular, cellular, and behavioral characterization of the acute and chronic effects of increased hippocampal Aβ$_{1–42}$ concentration, achieved through bilateral intra-hippocampal Aβ$_{1–42}$ injection in mice. We report that a single hippocampal Aβ$_{1–42}$ injection resulted in localized layer-specific alterations in the abundance of inflammatory- and vascular markers and phosphorylated tau, at the injection site. At all the time points examined post-injection (7–30 days) significant long-term spatial memory impairments were found in Aβ$_{1–42}$-injected mice compared to controls along with a significant neuronal cell loss in the str. pyramidale of the CA1 region. Our data suggest that inflammation and vascular disruption along with the local tau pathology observed in the CA1 region of the hippocampus might represent a

relevant, complex, and interactive combination of leading factors that synergistically contribute to the hippocampus-dependent spatial memory impairment observed in the $A\beta_{1-42}$-injected mice.

Pyramidal Cell Loss in the CA1 Hippocampal Region of $A\beta_{1-42}$-Injected Mice

We found a significant $A\beta_{1-42}$ mediated pyramidal cell loss by 7 days in the str. pyramidale of the CA1 region of the hippocampus despite finding of an earlier study that hippocampal cell loss was not observed until 14 and 28 days, and not at 7 days (Takuma et al., 2004). This delayed response might be explained if there was a lower concentration of misfolded Aβ, and thereby fewer aggregates, perhaps because the less aggregation-prone $A\beta_{1-40}$ was used. Although extrapolation of findings from rodent models to human AD must be made with caution, the excitatory pyramidal cell loss observed here does occur in late-stage AD in humans (Rossler et al., 2002) and, was at a relatively late outcome in our study as well.

The neurotoxic effect induced by high concentrations of $A\beta_{1-42}$ observed in this study likely arose from a combination of factors, including damage from oxidative stress (Behl et al., 1995), activation of glial cells (Farfara et al., 2008), changes in intracellular Ca^{2+} concentrations and mitochondrial dysfunction (Arbel-Ornath et al., 2017). Aβ-induced apoptosis is likely mediated by the caspase-3-apoptotic cascade (Takuma et al., 2004; Brouillette et al., 2012; Vinnakota et al., 2020). $A\beta_{1-42}$-induced cell death might also result from oxidative stress and the generation of oxidative modifications to lipid and protein in the cell—the presence of intracerebral $A\beta_{1-42}$ in rats is associated with increased levels of oxidized proteins in the rat hippocampus (Boyd-Kimball et al., 2005). $A\beta_{1-42}$-induced activation of glial cells and the generation of pro-inflammatory cytokines may also contribute to neurodegeneration *in vivo* (Farfara et al., 2008). Cell loss induced by hippocampal injection of $A\beta_{1-42}$ in mice has been prevented by the administration of transforming growth factor (TGF)-β1, an immunosuppressive cytokine, which prevents glial activation and accumulation of $A\beta_{1-42}$ (Chen et al., 2015). In the present study, the significant local upregulation of activated microglia and reactive astrocytes that were observed in the $A\beta_{1-42}$-injected mice might also partially be responsible for the neural cell loss.

Tau Pathology-Related Changes in $A\beta_{1-42}$-Injected Mice

We report locally increased tau hyperphosphorylation by 30 days after $A\beta_{1-42}$ injection in the str. oriens, str. pyramidale, and str. radiatum of the CA1 region of the hippocampus. Microglial activation seems to precede both tau hyperphosphorylation (Yoshiyama et al., 2007) and NFT formation (Maphis et al., 2016) and this might explain why, despite other changes, there is no p-tau pathology at day 3 after injection of $A\beta_{1-42}$. The mechanism by which Aβ induces the activation of p-tau-dependent degeneration pathways in the cell has been widely investigated (Hurtado et al., 2010; Hu et al., 2014; Bennett et al., 2017). Hu et al. (2014) provide support for our conclusions as they demonstrated intra-hippocampal injection of aggregation susceptible $A\beta_{1-42}$, but not $A\beta_{1-40}$, in mice is responsible for the subsequent p-tau pathology of cell loss (Hu et al., 2014). Microglia may regulate tau phosphorylation through the microglial-specific fractalkine receptor (CX3CR1; Bhaskar et al., 2010). The ligand CX3CL1 is by contrast exclusively expressed by neurons and so neuron-microglia crosstalk likely precedes the p-tau pathology in AD. Indeed, disruption of the CX3CL1-CX3CR1 association has been shown to have a neuroprotective effect in a triple Tg AD mouse model (Fuhrmann et al., 2010).

Apart from contributions to both neuronal cell and synapse loss in the AD brain, p-tau pathology affects the generation of hippocampal theta oscillations, underlying the dysfunctional network circuitry in a triple Tg AD mouse model. A recent study reported that early tau pathology in the triple Tg AD mouse model resulted in a reduction in theta oscillations and overall excitability in the CA1 region of the hippocampus; perhaps as a compensatory mechanism for the prevention of Aβ-induced NMDA-mediated overexcitation (Mondragón-Rodríguez et al., 2018). Additionally, the accumulation of p-tau in parvalbumin-positive interneurons may also influence the changes in hippocampal activity and functionality (Soler et al., 2017). The tau pathology observed in the hippocampus and the activation of microglia might be one of the factors contributing to neurotoxicity and pyramidal cell loss in the CA1 region. While activation of microglia was observed further away from the injection site 3-day post $A\beta_{1-42}$ injection, long-distance spreading from the injection site of the p-tau protein along the CA1 region was not found, indicating a longer-term activation of microglia might be required to trigger p-tau pathology. At day 30, p-tau correlates with the number of activated astrocytes and microglia at the injection site, but not at day 3 or adjacent to the injection site at day 30 where we did not observe activation of these cells.

Inflammatory Changes in $A\beta_{1-42}$-Injected Mice

$A\beta_{1-42}$-induced inflammatory responses were confirmed by the local up-regulation of GFAP levels at day 3, as well as up-regulation of GFAP and Iba-1 levels by day 30, in $A\beta_{1-42}$-injected mice compared with controls. Whereas control mice displayed sparse resting astrocytes, $A\beta_{1-42}$-injected mice had an increased number of astrocytes with highly reactive morphologies depicted by numerous branching, elongated processes, and hypertrophic cell bodies. Astrogliosis, observable at day 3 and still present by day 30, occurred in the absence of significant increases in the immunoreactivity of the chemotactic factors IP-10 and MCP-1. Some studies have shown MCP-1 labeling near senile Aβ plaques, as well as reactive astrocytes expressing IP-10 in AD (McLarnon, 2012). Therefore, we hypothesize that the local acute inflammation following a single $A\beta_{1-42}$ injection might not be sufficient to trigger the detectable production of chemotactic factors in the mouse hippocampus,

as chemotactic factors in AD have been observed only during chronic neuroinflammation (McLarnon, 2012).

The activation of astrocytes seen on day 3 at the injection site was not maintained at an adjacent location until day 30. A previous study of Aβ-injection in a rat model showed that significantly elevated GFAP levels were observed 1 day after soluble Aβ injection, but not at day 30 (Weldon et al., 1998). We hypothesize that the system might be self-regulating with compensatory mechanisms for the inflammatory process in the proximity of the injection site and that acute astrocyte activation after $A\beta_{1-42}$ injection could be transient. Activated astrocytes surrounding and isolating Aβ aggregates might represent the beginning of the Aβ clearance. On the other hand, the observed microglia activation responses on day 3 and day 30 post-injection had also occurred, which implies a phagocytic role for the microglia after the $A\beta_{1-42}$ injection. Relationships between Aβ, neurons, astrocytes, and microglia in the AD brain are complex and should be further investigated.

Vascular Changes in $A\beta_{1-42}$-Injected Mice

$A\beta_{1-42}$-injected mice also displayed signs of early vascular dysfunction by day 3 as revealed by the up-regulation of the endothelial cell marker CD31 in the str. radiatum of the CA1 region of the hippocampus. Consistent with this, early endothelial cell dysfunction has already been seen in other mouse models of AD (Lee et al., 2018a,b) and also in AD patients (Kelleher and Soiza, 2013), suggesting early alterations in blood flow regulation and in BBB permeability. Aβ-mediated increase in reactive oxygen species generation could lead to endothelial cell dysfunction through the alteration of endothelial tight junctions (Carrano et al., 2011). The acute up-regulation of the CD31 levels seen in this study might play a role in counteracting early Aβ-mediated effects on the endothelial cell and/or be involved with an early inflammatory process around the BBB. At this stage, the beginning of a disruptive process might affect BBB integrity.

Importantly, the early vascular dysfunction seen in $A\beta_{1-42}$-injected mice is maintained up to day 30, and at this time point, CD31 labeling intensity was increased in the str. pyramidale and str. radiatum of the CA1 region of the hippocampus. In contrast to our results, reduced CD31 density was observed in 9-month-old Tg APP mice (Lee et al., 2018b), and Religa and colleagues demonstrated an inverse correlation between the number of plaques and CD31-labeled vessel density, which indicates that $A\beta_{1-42}$ destroys the integrity of the BBB. They further suggested that $A\beta_{1-42}$ led to apoptosis of endothelial and smooth muscle cells in AD patients and Tg TCRND8 APP mice (Religa et al., 2013). This apparent conflict with our findings might be resolved if the localized up-regulation of CD31 we observed is a compensatory molecular mechanism to re-establish homeostasis of the BBB, and to compensate for the loss of endothelial cells in cerebral capillaries during AD. Interestingly, tau overexpression affected endothelial cell functionality, as well as inducing vascular remodeling in a Tg AD mouse model (Bennett et al., 2018). Thus, local up-regulation of p-tau levels at the injection site in the present study may contribute to the dysfunction of endothelial cells in the BBB of $A\beta_{1-42}$-injected mice. Indeed, p-tau levels show a positive correlation with CD31 levels on day 30 after $A\beta_{1-42}$ injection.

Essential for the maintenance of vascular integrity in the brain, α-SMA has been extensively investigated in the context of AD pathogenesis. Here we report up-regulated α-SMA levels at the injection site in the CA1 region of the hippocampus in $A\beta_{1-42}$-injected mice at day 30 post-injection. Furthermore, this up-regulation of α-SMA spread along the entire CA1 region. A lower degree of α-SMA immunostaining was found in the blood vessels of AD patients compared to controls (Ervin et al., 2004) but also increased expression of α-SMA in preclinical AD cases (Ervin et al., 2004). Consistent with our results, another AD mouse model was found to express high α-SMA immunostaining near Aβ plaques in the blood vessels in the cortex (Hutter-Schmid and Humpel, 2016). In preliminary studies, we have also detected an increase in α-SMA immunostaining in the middle temporal cortex of AD cases using tissue microarray methods (Austria et al., unpublished). It has been shown that smooth muscle cells undergo degeneration and atrophy during AD (Farkas and Luiten, 2001); therefore, the up-regulated α-SMA levels observed here might be an indicator of a systemic compensatory mechanism. Alternatively, since α-SMA regulates blood vessel contraction, its expression may be up-regulated to counteract any early dysfunction in blood flow occurring following $A\beta_{1-42}$'injection.

In the present study, up-regulated fibrinogen labeling at day 3 post-injection was also observed in the str. oriens of the CA1 region of the hippocampus. Three Tg AD mouse models, TgCRND8, PDAPP, and Tg2576, also have high levels of fibrinogen (Paul et al., 2007); confirming the contribution of fibrinogen to the pathology of AD, mostly *via* inflammatory processes. In agreement with this, in mouse models overexpressing APP in which fibrinogen was eliminated, microgliosis was found to be reduced (Paul et al., 2007). Fibrinogen infiltration and microglial reactivity have also been observed in $A\beta_{1-42}$ intrahippocampal injected rodent brains and the human AD brain (Ryu and McLarnon, 2009). Indeed, increased fibrinogen density at day 3 shows a positive correlation with increased astrogliosis and microglia activation at day 3 after $A\beta_{1-42}$ injection. Furthermore, increased fibrinogen deposition in $A\beta_{1-42}$-injected mice might promote microvascular permeability through a negative effect on endothelial tight junction proteins (Tyagi et al., 2008), resulting in the accumulation of fibrinogen outside of circulation. Another possible mechanism by which fibrinogen could mediate BBB disruption is by affecting the accumulation and/or clearance process of Aβ in the vessels. Indeed, when fibrinogen levels were reduced in TgCRND8 AD mice, cerebral amyloid angiopathy was significantly diminished and reduced fibrinogen levels were linked to significant improvement in spatial memory (Cortes-Canteli et al., 2010). This finding indicates that one of the multiple factors associated with cognitive decline in the present AD mouse model could be the infiltration of fibrinogen into the hippocampal areas of the brain of $A\beta_{1-42}$-injected mice, with the subsequent associated pathological events.

Cognitive and Behavioral Changes in $A\beta_{1-42}$-Injected Mice

A large number of Aβ-injected AD rodent models have demonstrated cognitive decline after infusion of the neurotoxic Aβ into rodent brains (Yamada et al., 1999; Nakamura et al., 2001; Tohda et al., 2003; Tsukuda et al., 2009; Takeda et al., 2014; Sadigh-Eteghad et al., 2015; Faucher et al., 2016). Spatial memory impairment is likely a result of the effects of increased Aβ concentrations at localized sites, confirmed by Aβ administration through both the i.c.v (Tsukuda et al., 2009; Kasza et al., 2017; Schmid et al., 2017) and hippocampal routes (Xuan et al., 2012).

Much evidence has shown that spatial memory impairment is caused by Aβ deposition and the subsequent synaptic dysfunction, among other Aβ-mediated effects, in the hippocampal area (Balducci et al., 2010). Exploration of novel objects is a critical approach to assess hippocampal-dependent spatial memory in AD rodent models. Our results demonstrate that $A\beta_{1-42}$-injected mice showed hippocampal-dependent spatial memory impairment, as indicated by the results of the NOA, NOR and MWM tests on days 3 (Yeung et al., 2020b) and 30 post-injection, respectively. Previous studies have reported cognitive decline after Aβ infusion into rodent brains, assessed by NOR. $A\beta_{1-42}$-mediated impairment of long-term spatial recognition memory was reported following a single injection of neurotoxic $A\beta_{1-42}$ (i.c.v) into male C57BL/6 mice (Balducci et al., 2010). Takeda and colleagues found only very transient cognitive impairment after infusion of $A\beta_{1-42}$ into the DG region of rats using the NOR test, and it was found to be associated with decreased long-term potentiation (LTP; Takeda et al., 2014). The short duration of the cognitive impairment indicates that the Aβ-mediated effect might vary among different areas of the hippocampus. Unlike this finding, our results demonstrated long-lasting $A\beta_{1-42}$ effects on cognition, with the MWM test performed 20 days after the injection showing long-term spatial memory impairment in $A\beta_{1-42}$-injected mice.

The MWM test is one of the most robust and most popular cognitive tests to assess hippocampal-dependent spatial memory (Tsukuda et al., 2009; Xuan et al., 2012; Esfandiary et al., 2015). We demonstrated that $A\beta_{1-42}$-injected mice spent significantly less time in the platform quadrant than control mice during the last 2 days of the MWM test. In agreement with our findings, Xuan and colleagues also reported spatial memory impairment (using the MWM test) following the injection of $A\beta_{1-40}$ into the dentate gyrus of the hippocampus of rats (Xuan et al., 2012). They observed astrogliosis and microgliosis in the hippocampus of the $A\beta_{1-40}$-injected rats, consistent with our results in $A\beta_{1-42}$-injected mice. Cognitive deficits were also demonstrated in $A\beta_{25-35}$-injected mice (i.c.v administration) by the MWM test. Esfandiary and colleagues also demonstrated spatial-memory impairment (assessed by the MWM test) in an AD mouse model in which $A\beta_{1-42}$ was intra-hippocampally injected into the CA1 region of the mice. In agreement with our findings, this study failed to demonstrate impairment in non-spatial memory, according to assessment with the passive avoidance test (Esfandiary et al., 2015). $A\beta_{1-42}$ injection (i.c.v) in rats also resulted in cognitive deficits according to the MWM test (Zhang et al., 2015).

We did not find significant short-term spatial memory deficits with the YM test in $A\beta_{1-42}$-injected mice, although there was a trend towards decreased alternations. Huh et al. (2014) found the percentage of alternations in mice where the DG was intra-hippocampally injected with $A\beta_{1-42}$ was significantly lower than in the control group. Other studies have confirmed this with $A\beta_{1-42}$-i.c.v injected mice (Yan et al., 2001) and rats (Zhang et al., 2015). Thus, the YM test might be a valid method to assess cognitive impairment in short-term memory induced by $A\beta_{1-42}$ in rodent models.

In our study, no significant deficits were observed in non-spatial memory in the $A\beta_{1-42}$-injected mice, utilizing the passive avoidance test (Esfandiary et al., 2015). These findings imply that the hippocampus might not be overly involved with non-spatial memory processes (Cave and Squire, 1991) and that Aβ affects only hippocampal-dependent memory processes. The passive avoidance test is used to assess a type of contextual memory which partly involves processing in the CA3 region of the hippocampus (Daumas et al., 2004) but our model is based on a single $A\beta_{1-42}$ injection into the CA1 region, and that the CA1 area might be more critical in recognizing the novelty or familiarity of an object rather than contextual related-memories (Nakazawa et al., 2004; Daumas et al., 2005). This type of non-spatial memory likely remains unaffected in our experiments. An earlier study found that soon after $A\beta_{1-42}$ i.c.v injection (day 1 and 7), mice exhibited deteriorated long-term non-spatial memory (Yan et al., 2001). Differences in the injected brain area, along with slight variations in the behavioral task design, might be factors that can potentially contribute to the divergence of results to those found in the literature.

The observed short-term spatial memory deficits correlate with p-tau, inflammatory and vascular pathology. Cognitive performance of $A\beta_{1-42}$-injected mice showed a negative correlation with p-tau density, the number of activated astrocytes and microglia, and CD31 density. Most likely all these pathological changes are contributing factors to the cognitive deficits observed in these mice along with other molecular and cellular deficits. Short-term spatial memory deficits at day 3 occur before any significant neuronal loss (Yeung et al., 2020a), suggesting that all these pathological changes are sufficient to impair neural activity and information processing. The hippocampal $A\beta_{1-42}$ injection in our study likely results in dysfunctional neural networks within the CA1, CA3 and the dentate gyrus, as there are widespread and complex interconnections within these hippocampal regions (Amaral et al., 2007). Likewise, it is well known that tau and amyloid can propagate throughout synaptically connected networks in the hippocampus (Cirrito et al., 2005; de Calignon et al., 2012). The physiological changes induced directly by $A\beta_{1-42}$ throughout the hippocampus and other brain areas have been extensively studied but the link of network dysfunction with the complex pathological and behavioral changes needs to be further explored in future experiments.

In summary, our study shows that a single Aβ injection can reproduce aspects of the molecular, cellular, and vascular changes occurring in the AD human brain and can lead to cognitive deficits. We have demonstrated that not only classic Aβ and tau pathology features of AD contribute to the cognitive decline, but that neuroinflammation and vascular pathology may also play a key role in hippocampal-memory and learning deficits in AD.

DATA AVAILABILITY STATEMENT

All datasets presented in this study are included in the article.

ETHICS STATEMENT

The animal study was reviewed and approved by the University of Otago Animal Ethics Committee and the University of Auckland Animal Ethics Committee.

AUTHOR CONTRIBUTIONS

BC-F, TC, TP, SW, KP, and AK: performed research. BC-F, TC, TP, SW, KP, JB, and AK: analyzed data. BC-F, TC, WT, HW, RF, and AK: wrote the article. WT, MD, and AK: designed research. MD, RF, and AK: funding acquisition. AK: project administration. WT, HW, RF, and AK: supervision. All authors contributed to the article and approved the submitted version.

FUNDING

This work was supported by Alzheimer's New Zealand Charitable Trust (AK; 3720863); Alzheimer's New Zealand (AK; 3718869); Freemasons New Zealand (AK; 3719321); Aotearoa Foundation, Centre for Brain Research, University of Auckland (AK; 3705579); Brain Research New Zealand (BC-F, HW, RF, AK; 3710638); Health Research Council of New Zealand (MD, RF, HW; 3627373), Neurological Foundation of New Zealand (AK and TP; 848010).

ACKNOWLEDGMENTS

We thank Kristina Hubbard, Jacqueline Ross and Marika Eszes for their excellent work and assistance, and members of the Hercus Taieri Resource Unit, University of Otago, and Vernon Jansen Unit, University of Auckland also for their excellent work.

REFERENCES

Amaral, D. G., Scharfman, H. E., and Lavenex, P. (2007). The dentate gyrus: fundamental neuroanatomical organization (dentate gyrus for dummies). *Prog. Brain Res.* 163, 3–22. doi: 10.1016/S0079-6123(07)63001-5

Arbel-Ornath, M., Hudry, E., Boivin, J. R., Hashimoto, T., Takeda, S., Kuchibhotla, K. V., et al. (2017). Soluble oligomeric amyloid-β induces calcium dyshomeostasis that precedes synapse loss in the living mouse brain. *Mol. Neurodegener.* 12:27. doi: 10.1186/s13024-017-0169-9

Arriagada, P. V., Growdon, J. H., Hedley-Whyte, E. T., and Hyman, B. T. (1992). Neurofibrillary tangles but not senile plaques parallel duration and severity of Alzheimer's disease. *Neurology* 42, 631–639. doi: 10.1212/wnl.42.3.631

Balducci, C., Beeg, M., Stravalaci, M., Bastone, A., Sclip, A., Biasini, E., et al. (2010). Synthetic amyloid-β oligomers impair long-term memory independently of cellular prion protein. *Proc. Natl. Acad. Sci. U S A* 107, 2295–2300. doi: 10.1073/pnas.0911829107

Baluchnejadmojara, D. T., Mohamadi-Zarch, S., and Roghani, M. (2019). Safranal, an active ingredient of saffron, attenuates cognitive deficits in amyloid β-induced rat model of Alzheimer's disease: underlying mechanisms metabolic brain disease. *Metab. Brain Dis.* 34, 1747–1759. doi: 10.1073/pnas.0911829107

Behl, C., Widmann, M., Trapp, T., and Holsboer, F. (1995). 17-β estradiol protects neurons from oxidative stress-induced cell death *in vitro*. *Biochem. Biophys. Res. Commun.* 216, 473–482. doi: 10.1006/bbrc.1995.2647

Bekris, L. M., Yu, C.-E., Bird, T. D., and Tsuang, D. W. (2010). Genetics of Alzheimer disease. *J. Geriatr. Psychiatry Neurol.* 23, 213–227. doi: 10.1177/0891988710383571

Bennett, R. E., DeVos, S. L., Dujardin, S., Corjuc, B., Gor, R., Gonzalez, J., et al (2017). Enhanced tau aggregation in the presence of amyloid-β. *Am. J. Pathol.* 187, 1601–1612. doi: 10.1016/j.ajpath.2017.03.011

Bennett, R. E., Robbins, A. B., Hu, M., Cao, X., Betensky, R. A., Clark, T., et al. (2018). Tau induces blood vessel abnormalities and angiogenesis-related gene expression in P301L transgenic mice and human Alzheimer's disease. *Proc. Natl. Acad. Sci. U S A* 115:E1289. doi: 10.1073/pnas.1710329115

Bettcher, B. M., Neuhaus, J., Wynn, M. J., Elahi, F. M., Casaletto, K. B., Saloner, R., et al. (2019). Increases in a pro-inflammatory chemokine, MCP-1, are related to decreases in memory over time. *Front. Aging Neurosci.* 11, 25–25. doi: 10.3389/fnagi.2019.00025

Bhaskar, K., Konerth, M., Kokiko-Cochran, O. N., Cardona, A., Ransohoff, R. M., and Lamb, B. T. (2010). Regulation of tau pathology by the microglial fractalkine receptor. *Neuron* 68, 19–31. doi: 10.1016/j.neuron.2010.08.023

Boche, D., and Nicoll, J. A. R. (2020). Understanding cause and effect in Alzheimer's pathophysiology: implications for clinical trials. *Neuropathol. Appl. Neurobiol.* doi: 10.1111/nan.12642.

Boche, D., Perry, V. H., and Nicoll, J. A. R. (2013). Review: activation patterns of microglia and their identification in the human brain. *Neuropathol. Appl. Neurobiol.* 39, 3–18. doi: 10.1111/nan.12011

Boyd-Kimball, D., Sultana, R., Poon, H. F., Lynn, B., Casamenti, F., Pepeu, G., et al. (2005). Proteomic identification of proteins specifically oxidized by intracerebral injection of amyloid-β-peptide (1–42) into rat brain: implications for Alzheimer's disease. *Neuroscience* 132, 313–324. doi: 10.1016/j.neuroscience.2004.12.022

Brouillette, J., Caillierez, R., Zommer, N., Alves-Pires, C., Benilova, I., Blum, D., et al. (2012). Neurotoxicity and memory deficits induced by soluble low-molecular-weight amyloid-β_{1-42} oligomers are revealed *in vivo* by using a novel animal model. *J. Neurosci.* 32, 7852–7861. doi: 10.1523/jneurosci.5901-11.2012

Brun, A., and Englun, E. (1981). Regional pattern of degeneration in Alzheimer's disease: neuronal loss and histopathological grading. *Histopathology* 5, 549–564. doi: 10.1111/j.1365-2559.1981.tb01818.x

Calvo-Flores Guzmán, B., Kim, S., Chawdhary, B., Peppercorn, K., Tate, W. P., Waldvogel, H. J., et al. (2020). Amyloid-β_{1-42}-induced increase in GABAergic tonic conductance in mouse hippocampal CA1 pyramidal cells. *Molecules* 25:693.

Carrano, A., Hoozemans, J. J., van der Vies, S. M., Rozemuller, A. J., van Horssen, J., and de Vries, H. E. (2011). Amyloid Beta induces oxidative stress-mediated blood-brain barrier changes in capillary amyloid angiopathy. *Antioxid. Redox Signal.* 15, 1167–1178. doi: 10.1089/ars.2011.3895

Cave, C. B., and Squire, L. R. (1991). Equivalent impairment of spatial and nonspatial memory following damage to the human hippocampus. *Hippocampus* 1, 329–340. doi: 10.1002/hipo.450010323

Cetin, F., Yazihan, N., Dincer, S., and Akbulut, G. (2013). The effect of intracerebroventricular injection of beta amyloid peptide (1–42) on caspase-3 activity, lipid peroxidation, nitric oxide and NOS expression in young adult and aged rat brain. *Turk. Neurosurg.* 23, 144–150. doi: 10.5137/1019-5149.Jtn.5855-12.1

Chen, J.-H., Ke, K.-F., Lu, J.-H., Qiu, Y.-H., and Peng, Y.-P. (2015). Protection of TGF-β against neuroinflammation and neurodegeneration in Aβ1–42-induced

Alzheimer's disease model rats. *PLoS One* 10:e0116549. doi: 10.1371/journal.pone.0116549

Cirrito, J. R., Yamada, K. A., Finn, M. B., Sloviter, R. S., Bales, K. R., May, P. C., et al. (2005). Synaptic activity regulates interstitial fluid amyloid-beta levels *in vivo*. *Neuron* 48, 913–922. doi: 10.1016/j.neuron.2005.10.028

Conductier, G., Blondeau, N., Guyon, A., Nahon, J. L., and Rovere, C. (2010). The role of monocyte chemoattractant protein MCP1/CCL2 in neuroinflammatory diseases. *J. Neuroimmunol.* 224, 93–100. doi: 10.1016/j.jneuroim.2010.05.010

Cortes-Canteli, M., Paul, J., Norris, E. H., Bronstein, R., Ahn, H. J., Zamolodchikov, D., et al. (2010). Fibrinogen and β-amyloid association alters thrombosis and fibrinolysis: a possible contributing factor to Alzheimer's disease. *Neuron* 66, 695–709. doi: 10.1016/j.neuron.2010.05.014

Cortes-Canteli, M., Zamolodchikov, D., Ahn, H., Strickland, S., and Norris, E. (2012). Fibrinogen and altered hemostasis in Alzheimer's disease. *J. Alzheimers Dis.* 32, 599–608. doi: 10.3233/JAD-2012-120820

Daumas, S., Halley, H., and Lassalle, J.-M. (2004). Disruption of hippocampal CA3 network: effects on episodic-like memory processing in C57BL/6J mice. *Eur. J. Neurosci.* 20, 597–600. doi: 10.1111/j.1460-9568.2004.03484.x

Daumas, S., Halley, H., Francés, B., and Lassalle, J.-M. (2005). Encoding, consolidation and retrieval of contextual memory: differential involvement of dorsal CA3 and CA1 hippocampal subregions. *Learn. Mem.* 12, 375–382. doi: 10.1101/lm.81905

de Calignon, A., Polydoro, M., Suarez-Calvet, M., William, C., Adamowicz, D. H., Kopeikina, K. J., et al. (2012). Propagation of tau pathology in a model of early Alzheimer's disease. *Neuron* 73, 685–697. doi: 10.1016/j.neuron.2011.11.033

D'Hooge, R., and De Deyn, P. P. (2001). Applications of the Morris water maze in the study of learning and memory. *Brain Res. Brain Res. Rev.* 36, 60–90. doi: 10.1016/s0165-0173(01)00067-4

Drummond, E., and Wisniewski, T. (2017). Alzheimer's disease: experimental models and reality. *Acta Neuropathol.* 133, 155–175. doi: 10.1007/s00401-016-1662-x

Erickson, M. A., and Banks, W. A. (2013). Blood-brain barrier dysfunction as a cause and consequence of Alzheimer's disease. *J. Cereb. Blood Flow Metab.* 33, 1500–1513. doi: 10.1038/jcbfm.2013.135

Ervin, J. F., Pannell, C., Szymanski, M., Welsh-Bohmer, K., Schmechel, D. E., and Hulette, C. M. (2004). Vascular smooth muscle actin is reduced in Alzheimer disease brain: a quantitative analysis. *J. Neuropathol Exp. Neurol.* 63, 735–741. doi: 10.1093/jnen/63.7.735

Esfandiary, E., Karimipour, M., Mardani, M., Ghanadian, M., Alaei, H. A., Mohammadnejad, D., et al. (2015). Neuroprotective effects of *Rosa damascena* extract on learning and memory in a rat model of amyloid-β-induced Alzheimer's disease. *Adv. Biomed. Res.* 4:131. doi: 10.4103/2277-9175.161512

Facchinetti, R., Bronzuoli, M. R., and Scuderi, C. (2018). An animal model of Alzheimer disease based on the intrahippocampal injection of amyloid β-peptide (1–42). *Methods Mol. Biol.* 1727, 343–352. doi: 10.1007/978-1-4939-7571-6_25

Farfara, D., Lifshitz, V., and Frenkel, D. (2008). Neuroprotective and neurotoxic properties of glial cells in the pathogenesis of Alzheimer's disease. *J. Cell. Mol. Med.* 12, 762–780. doi: 10.1111/j.1582-4934.2008.00314.x

Farkas, E., and Luiten, P. G. (2001). Cerebral microvascular pathology in aging and Alzheimer's disease. *Prog. Neurobiol.* 64, 575–611. doi: 10.1016/s0301-0082(00)00068-x

Faucher, P., Mons, N., Micheau, J., Louis, C., and Beracochea, D. J. (2016). Hippocampal injections of oligomeric amyloid β-peptide (1–42) induce selective working memory deficits and long-lasting alterations of ERK signaling pathway. *Front. Aging Neurosci.* 7, 245–245. doi: 10.3389/fnagi.2015.00245

Franco, R., and Cedazo-Minguez, A. (2014). Successful therapies for Alzheimer's disease: why so many in animal models and none in humans? *Front. Pharmacol.* 5:146. doi: 10.3389/fphar.2014.00146

Fuhrer, T. E., Palpagama, T. H., Waldvogel, H. J., Synek, B. J. L., Turner, C., Faull, R. L., et al. (2017). Impaired expression of GABA transporters in the human Alzheimer's disease hippocampus, subiculum, entorhinal cortex and superior temporal gyrus. *Neuroscience* 351, 108–118. doi: 10.1016/j.neuroscience.2017.03.041

Fuhrmann, M., Bittner, T., Jung, C. K. E., Burgold, S., Page, R. M., Mitteregger, G., et al. (2010). Microglial Cx3cr1 knockout prevents neuron loss in a mouse model of Alzheimer's disease. *Nat. Neurosci.* 13, 411–413. doi: 10.1038/nn.2511

Glenn, J. A., Ward, S. A., Stone, C. R., Booth, P. L., and Thomas, W. E. (1992). Characterisation of ramified microglial cells: detailed morphology, morphological plasticity and proliferative capability. *J. Anat.* 180, 109–118.

Govindpani, K., Calvo-Flores Guzmán, B., Vinnakota, C., Waldvogel, H. J., Faull, R. L., and Kwakowsky, A. (2017). Towards a better understanding of GABAergic remodeling in Alzheimer's disease. *Int. J. Mol. Sci.* 18:1813. doi: 10.3390/ijms18081813

Govindpani, K., McNamara, L. G., Smith, N. R., Vinnakota, C., Waldvogel, H. J., Faull, R. L., et al. (2019). Vascular dysfunction in Alzheimer's disease: a prelude to the pathological process or a consequence of it? *J. Clin. Med.* 8:651. doi: 10.3390/jcm8050651

Govindpani, K., Vinnakota, C., Waldvogel, H. J., Faull, R. L., and Kwakowsky, A. (2020). Vascular dysfunction in Alzheimer's disease: a biomarker of disease progression and a potential therapeutic target. *Neural Regen. Res.* 15, 1030–1032. doi: 10.4103/1673-5374.270306

Hardy, J., and Selkoe, D. J. (2002). The amyloid hypothesis of Alzheimer's disease: progress and problems on the road to therapeutics. *Science* 297, 353–356. doi: 10.1126/science.1072994

Harris, S. S., Wolf, F., De Stooper, B., and Busche, M. A. (2020). Tipping the scales: peptide-dependent dysregulation of neural circuit dynamics in Alzheimer's disease. *Neuron* 107, 417–435. doi: 10.1016/j.neuron.2020.06.005.

Hillen, H. (2019). The beta amyloid dysfunction (BAD) hypothesis for Alzheimer's disease. *Front. Neurosci.* 13:1154. doi: 10.3389/fnins.2019.01154

Hu, X., Li, X., Zhao, M., Gottesdiener, A., Luo, W., and Paul, S. (2014). Tau pathogenesis is promoted by $A\beta_{1-42}$ but not $A\beta_{1-40}$. *Mol. Neurodegener.* 9:52. doi: 10.1186/1750-1326-9-52

Huang, Y., and Mucke, L. (2012). Alzheimer mechanisms and therapeutic strategies. *Cell* 148, 1204–1222.

Huber, C. M., Yee, C., May, T., Dhanala, A., and Mitchell, C. S. (2017). Cognitive decline in preclinical Alzheimer's disease: amyloid-β versus tauopathy. *J. Alzheimers Dis.* 61, 265–281. doi: 10.3233/JAD-170490

Huh, E., Kim, H. G., Park, H., Kang, M. S., Lee, B., and Oh, M. S. (2014). Houttuynia cordata improves cognitive deficits in cholinergic dysfunction Alzheimer's disease-like models. *Biomol. Ther.* 22, 176–183. doi: 10.4062/biomolther.2014.040

Hurtado, D. E., Molina-Porcel, L., Iba, M., Aboagye, A. K., Paul, S. M., Trojanowski, J. Q., et al (2010). Aβ accelerates the spatiotemporal progression of tau pathology and augments tau amyloidosis in an alzheimer mouse model. *Am. J. Pathol.* 177, 1977–1988. doi: 10.2353/ajpath.2010.100346.

Hutter-Schmid, B., and Humpel, C. (2016). Alpha-smooth muscle actin mRNA and protein are increased in isolated brain vessel extracts of Alzheimer mice. *Pharmacology* 98, 251–260. doi: 10.1159/000448007

Kamphuis, W., Mamber, C., Moeton, M., Kooijman, L., Sluijs, J. A., Jansen, A. H., et al. (2012). GFAP isoforms in adult mouse brain with a focus on neurogenic astrocytes and reactive astrogliosis in mouse models of Alzheimer disease. *PLoS One* 7:e42823. doi: 10.1371/journal.pone.0042823

Karran, E., Mercken, M., and De Strooper, B. (2011). The amyloid cascade hypothesis for Alzheimer's disease: an appraisal for the development of therapeutics. *Nat. Rev. Drug Discov.* 10, 698–712. doi: 10.1038/nrd3505

Kasza, Á., Penke, B., Frank, Z., Bozsó, Z., Szegedi, V., Hunya, Á., et al. (2017). Studies for improving a rat model of Alzheimer's disease: Icv administration of well-characterized β-amyloid 1–42 oligomers induce dysfunction in spatial memory. *Molecules* 22:2007. doi: 10.3390/molecules22112007

Kelleher, R. J., and Soiza, R. L. (2013). Evidence of endothelial dysfunction in the development of Alzheimer's disease: Is Alzheimer's a vascular disorder? *Am. J. Cardiovasc Dis.* 3, 197–226.

Klein, A. M., Kowall, N. W., and Ferrante, R. J. (1999). Neurotoxicity and oxidative damage of beta amyloid 1–42 versus beta amyloid 1–40 in the mouse cerebral cortex. *Ann. N Y Acad. Sci.* 893, 314–320. doi: 10.1111/j.1749-6632.1999.tb07845.x

Kruger, L., and Mandelkow, E. M. (2015). Tau neurotoxicity and rescue in animal models of human Tauopathies. *Curr Opin Neurobiol* 36, 52–58. doi: 10.1016/j.conb.2015.09.004

Kwakowsky, A., Calvo-Flores Guzman, B., Pandya, M., Turner, C., Waldvogel, H. J., and Faull, R. L. (2018). GABAA receptor subunit expression changes in the human Alzheimer's disease hippocampus, subiculum, entorhinal cortex and superior temporal gyrus. *J. Neurochem.* 145, 374–392. doi: 10.1111/jnc.14325

Kwakowsky, A., Potapov, K., Kim, S., Peppercorn, K., Tate, W. P., and Abraham, I. M. (2016). Treatment of beta amyloid 1–42 ($A\beta_{1-42}$)-induced basal forebrain cholinergic damage by a non-classical estrogen signaling activator *in vivo*. *Sci. Rep.* 6:21101. doi: 10.1038/srep21101

Kwakowsky, A., Waldvogel, H. J., and Faull, R. L. M. (2020). Therapeutic potential of a5 subunit containing GABAA receptors in Alzheimer's disease. *Neural Regener. Res.* 16:2021.

Lee, D., Cho, S. -J., Lim, H. J., Seok, J., Jo, C., Jo, S. A., et al. (2018a). Alteration of vascular endothelial cadherin in Alzheimer's disease patient and mouse model. *BioRxiv* 430140. doi: 10.1101/430140

Lee, W. J., Liao, Y. C., Wang, Y. F., Lin, I. F., Wang, S. J., and Fuh, J. L. (2018b). Plasma MCP-1 and cognitive decline in patients with Alzheimer's disease and mild cognitive impairment: a two-year follow-up study. *Sc.i Rep.* 8:1280. doi: 10.1038/s41598-018-19807-y

Lee, J. W., Lee, Y. K., Yuk, D. Y., Choi, D. Y., Ban, S. B., Oh, K. W., et al. (2008). Neuro-inflammation induced by lipopolysaccharide causes cognitive impairment through enhancement of beta-amyloid generation. *J. Neuroinflammation* 5, 37–37. doi: 10.1186/1742-2094-5-37

Leung, R., Proitsi, P., Simmons, A., Lunnon, K., Güntert, A., Kronenberg, D., et al. (2013). Inflammatory proteins in plasma are associated with severity of Alzheimer's disease. *PLoS One* 8:e64971. doi: 10.1371/journal.pone.0064971

Limon, A., Reyes-Ruiz, J. M., and Miledi, R. (2012). Loss of functional GABA(A) receptors in the Alzheimer diseased brain. *Proc. Natl. Acad. Sci. U S A* 109, 10071–10076. doi: 10.1073/pnas.1204606109

Liu, J., Gao, X., and Wu, Y. (2008). N-Methyl-*D*-aspartate receptors mediate excitotoxicity in amyloid beta-induced synaptic pathology of Alzheimer's disease. *Neuroembryol. Aging* 5, 134–143. doi: 10.1159/000193851

Llorian, M., Gooding, C., Bellora, N., Hallegger, M., Buckroyd, A., Wang, X., et al. (2016). The alternative splicing program of differentiated smooth muscle cells involves concerted non-productive splicing of post-transcriptional regulators. *Nucleic Acids Res.* 44, 8933–8950. doi: 10.1093/nar/gkw560

Maphis, N., Jiang, S., Xu, G., Kokiko-Cochran, O. N., Roy, S. M., Van Eldik, L. J., et al. (2016). Selective suppression of the α isoform of p38 MAPK rescues late-stage tau pathology. *Alzheimers Res. Ther.* 8:54. doi: 10.1186/s13195-016-0221-y

Marczynski, T. J. (1998). GABAergic deafferentation hypothesis of brain aging and Alzheimer's disease revisited. *Brain Res. Bull.* 45, 341–379. doi: 10.1016/s0361-9230(97)00347-x

Marín-Teva, J. L., Cuadros, M. A., Martín-Oliva, D., and Navascués, J. (2011). Microglia and neuronal cell death. *Neuron Glia Biol.* 7, 25–40. doi: 10.1017/s1740925x12000014

McLarnon, J. G. (2012). Microglial chemotactic signaling factors in Alzheimer's disease. *Am. J. Neurodegener Dis.* 1, 199–204.

Mondragón-Rodríguez, S., Salas-Gallardo, A., González-Pereyra, P., Macías, M., Ordaz, B., Peña-Ortega, F., et al. (2018). Phosphorylation of Tau protein correlates with changes in hippocampal theta oscillations and reduces hippocampal excitability in Alzheimer's model. *J. Biol. Chem.* 293, 8462–8472. doi: 10.1074/jbc.RA117.001187

Mudò, G., Frinchi, M., Nuzzo, D., Scaduto, P., Plescia, F., Massenti, M. F., et al. (2019). Anti-inflammatory and cognitive effects of interferon-β1a (IFNβ1a) in a rat model of Alzheimer's disease. *J. Neuroinflammation* 16:44. doi: 10.1186/s12974-019-1417-4.

Muoio, V., Persson, P. B., and Sendeski, M. M. (2014). The neurovascular unit – concept review. *Acta Physiol.* 210, 790–798. doi: 10.1111/apha.12250

Nakamura, S., Murayama, N., Noshita, T., Annoura, H., and Ohno, T. (2001). Progressive brain dysfunction following intracerebroventricular infusion of beta1–42-amyloid peptide. *Brain Res.* 912, 128–136. doi: 10.1016/s0006-8993(01)02704-4

Nakazawa, K., McHugh, T. J., Wilson, M. A., and Tonegawa, S. (2004). NMDA receptors, place cells and hippocampal spatial memory. *Nat. Rev. Neurosci.* 5, 361–372. doi: 10.1038/nrn1385

Navarro, V., Sanchez-Mejias, E., Jimenez, S., Muñoz-Castro, C., Sanchez-Varo, R., Davila, J. C., et al. (2018). Microglia in Alzheimer's disease: activated, dysfunctional or degenerative. *Front. Aging Neurosci.* 10:140. doi: 10.3389/fnagi.2018.00140

Nelson, A. R., Sweeney, M. D., Sagare, A. P., and Zlokovic, B. V. (2016). Neurovascular dysfunction and neurodegeneration in dementia and Alzheimer's disease. *Biochim. Biophys. Acta* 1862, 887–900. doi: 10.1016/j.bbadis.2015.12.016

Nicole, O., Hadzibegovic, S., Gajda, J., Bontempi, B., Bem, T., and Meyrand, P. (2016). Soluble amyloid beta oligomers block the learning-induced increase in hippocampal sharp wave-ripple rate and impair spatial memory formation. *Sci. Rep.* 6:22728. doi: 10.1038/srep22728

Ohno, M., Cole, S. L., Yasvoina, M., Zhao, J., Citron, M., Berry, R., et al. (2007). BACE1 gene deletion prevents neuron loss and memory deficits in 5XFAD APP/PS1 transgenic mice. *Neurobiol. Dis.* 26, 134–145. doi: 10.1016/j.nbd.2006.12.008

Ohno, M., Sametsky, E. A., Younkin, L. H., Oakley, H., Younkin, S. G., Citron, M., et al. (2004). BACE1 deficiency rescues memory deficits and cholinergic dysfunction in a mouse model of Alzheimer's disease. *Neuron* 41, 27–33. doi: 10.1016/s0896-6273(03)00810-9

Palpagama, T. H., Sagniez, M., Kim, S., Waldvogel, H. J., Faull, R. L., and Kwakowsky, A. (2019a). $GABA_A$ receptor subunit expression is well preserved in the aged mouse hippocampus. *eNeuro*. 0496-18. –. doi: 10.1523/ENEURO.0496-18.2019

Palpagama, H. T., Waldvogel, H. J., Faull, R. L., and Kwakowsky, A. (2019b). The role of microglia and astrocytes in Huntington's disease. *Front. Mol. Neurosci.* 12:258. doi: 10.3389/fnmol.2019.00258

Pandya, M., Palpagama, T. H., Turner, C., Waldvogel, H. J., Faull, R. L., and Kwakowsky, A. (2019). Sex- and age-related changes in GABA signaling components in the human cortex. *Biol. Sex Differ.* 10:5. doi: 10.1186/s13293-018-0214-6

Paul, J., Strickland, S., and Melchor, J. P. (2007). Fibrin deposition accelerates neurovascular damage and neuroinflammation in mouse models of Alzheimer's disease. *J. Exp. Med.* 204, 1999–2008. doi: 10.1084/jem.20070304

Pritchard, S. M., Dolan, P. J., Vitkus, A., and Johnson, G. V. (2011). The toxicity of tau in Alzheimer disease: turnover, targets and potential therapeutics. *J. Cell. Mol. Med.* 15, 1621–1635. doi: 10.1111/j.1582-4934.2011.01273.x

Puzzo, D., Lee, L., Palmeri, A., Calabrese, G., and Arancio, O. (2014). Behavioral assays with mouse models of Alzheimer's disease: practical considerations and guidelines. *Biochem. Pharmacol.* 88, 450–467. doi: 10.1016/j.bcp.2014.01.011

Religa, P., Cao, R., Religa, D., Xue, Y., Bogdanovic, N., Westaway, D., et al. (2013). VEGF significantly restores impaired memory behavior in Alzheimer's mice by improvement of vascular survival. *Sci. Rep.* 3:2053. doi: 10.1038/srep02053

Rissman, R. A., and Mobley, W. C. (2011). Implications for treatment: GABAA receptors in aging, down syndrome and Alzheimer's disease. *J. Neurochem.* 117, 613–622. doi: 10.1111/j.1471-4159.2011.07237.x

Rossler, M., Zarski, R., Bohl, J., and Ohm, T. G. (2002). Stage-dependent and sector-specific neuronal loss in hippocampus during Alzheimer's disease. *Acta Neuropathol.* 103, 363–369. doi: 10.1007/s00401-001-0475-7

Ryu, J. K., and McLarnon, J. G. (2009). A leaky blood-brain barrier, fibrinogen infiltration and microglial reactivity in inflamed Alzheimer's disease brain. *J. Cell. Mol. Med.* 13, 2911–2925. doi: 10.1111/j.1582-4934.2008.00434.x

Sadigh-Eteghad, S., Mahmoudi, J., Babri, S., and Talebi, M. (2015). Effect of alpha-7 nicotinic acetylcholine receptor activation on beta-amyloid induced recognition memory impairment. Possible role of neurovascular function. *Acta Cir. Bras.* 30, 736–742. doi: 10.1590/S0102-86502015011000003

Schmid, S., Jungwirth, B., Gehlert, V., Blobner, M., Schneider, G., Kratzer, S., et al. (2017). Intracerebroventricular injection of beta-amyloid in mice is associated with long-term cognitive impairment in the modified hole-board test. *Behav. Brain Res.* 324, 15–20. doi: 10.1016/j.bbr.2017.02.007

Soler, H., Dorca-Arévalo, J., González, M., Rubio, S. E., Ávila, J., Soriano, E., et al. (2017). The GABAergic septohippocampal connection is impaired in a mouse model of tauopathy. *Neurobiol. Aging* 49, 40–51. doi: 10.1016/j.neurobiolaging.2016.09.006

Soto-Rojas, L. O., de la Cruz-López, F., Torres, M. A. O., Viramontes-Pintos, A., del Carmen Cárdenas-Aguayo, M., Meraz-Ríos, M. A., et al. (2015). Neuroinflammation and alteration of the blood-brain barrier in Alzheimer's disease. In Alzheimer's Disease-Challenges for the Future: IntechOpen. doi: 10.5772/60024

Souchet, B., Audrain, M., Billoir, B., Lecanu, L., Tada, S., Braudeau, J., et al. (2018). Is it time to rethink the Alzheimer's disease drug development strategy by targeting its silent phase? *Neural Regen. Res.* 13, 224–225. doi: 10.4103/1673-5374.226389

Takeda, A., Nakamura, M., Fujii, H., Uematsu, C., Minamino, T., Adlard, P. A., et al. (2014). Amyloid β-mediated Zn^{2+} influx into dentate granule cells transiently induces a short-term cognitive deficit. *PLoS One* 9:e115923. doi: 10.1371/journal.pone.0115923

Takuma, H., Tomiyama, T., Kuida, K., and Mori, H. (2004). Amyloid beta peptide-induced cerebral neuronal loss is mediated by caspase-3 *in vivo*. *J. Neuropathol. Exp. Neurol.* 63, 255–261. doi: 10.1093/jnen/63.3.255

Tohda, C., Tamura, T., and Komatsu, K. (2003). Repair of amyloid β(25–35)-induced memory impairment and synaptic loss by a Kampo formula, Zokumei-to. *Brain Res.* 990, 141–147. doi: 10.1016/S0006-8993(03)03449-8

Tsukuda, K., Mogi, M., Iwanami, J., Min, L. J., Sakata, A., Jing, F., et al. (2009). Cognitive deficit in amyloid-beta-injected mice was improved by pretreatment with a low dose of telmisartan partly because of peroxisome proliferator-activated receptor-gamma activation. *Hypertension* 54, 782–787. doi: 10.1161/hypertensionaha.109.136879

Tyagi, N., Roberts, A. M., Dean, W. L., Tyagi, S. C., and Lominadze, D. (2008). Fibrinogen induces endothelial cell permeability. *Mol. Cell. Biochem.* 307, 13–22. doi: 10.1007/s11010-007-9579-2

van de Haar, H. J., Jansen, J. F. A., van Osch, M. J. P., van Buchem, M. A., Muller, M., Wong, S. M., et al. (2016). Neurovascular unit impairment in early Alzheimer's disease measured with magnetic resonance imaging. *Neurobiol. Aging* 45, 190–196. doi: 10.1016/j.neurobiolaging.2016.06.006

Vinnakota, C., Govondpani, K., Tate, W. P., Peppercorn, K., Aneka, P. V., Waldvogel, H. J., et al. (2020). An α5 $GABA_A$ receptor inverse agonist, α5IA, attenuates amyloid beta-induced neuronal death in mouse hippocampal cultures. *Int. J. Mol. Sci.* 21:3284. doi: 10.3390/ijms21093284

Wang, W., Nguyen, L. T. T., Burlak, C., Chegini, F., Guo, F., Chataway, T., et al. (2016). Caspase-1 causes truncation and aggregation of the Parkinson's disease-associated protein α-synuclein. *Proc. Natl. Acad. Sci.* 113, 9587–9592. doi: 10.1073/pnas.1610099113

Weldon, D. T., Rogers, S. D., Ghilardi, J. R., Finke, M. P., Cleary, J. P., O'Hare, E., et al. (1998). Fibrillar beta-amyloid induces microglial phagocytosis, expression of inducible nitric oxide synthase and loss of a select population of neurons in the rat CNS *in vivo*. *J. Neurosci.* 18, 2161–2173. doi: 10.1523/JNEUROSCI.18-06-02161.1998

Wennström, M., and Nielsen, H. M. (2012). Cell adhesion molecules in Alzheimer's disease. *Degener. Neurol. Neuromuscul. Dis.* 2, 65–77. doi: 10.2147/dnnd.S19829

Wilhelmsson, U., Bushong, E. A., Price, D. L., Smarr, B. L., Phung, V., Terada, M., et al. (2006). Redefining the concept of reactive astrocytes as cells that remain within their unique domains upon reaction to injury. *Proc. Natl. Acad. Sci. U S A* 103, 17513–17518. doi: 10.1073/pnas.0602841103

Wyssenbach, A., Quintela, T., Llavero, F., Zugaza, J. L., Matute, C., and Alberdi, E. (2016). Amyloid β-induced astrogliosis is mediated by β1-integrin *via* NADPH oxidase 2 in Alzheimer's disease. *Aging Cell* 15, 1140–1152. doi: 10.1111/acel.12521

Xia, M. Q., Bacskai, B. J., Knowles, R. B., Qin, S. X., and Hyman, B. T. (2000). Expression of the chemokine receptor CXCR3 on neurons and the elevated expression of its ligand IP-10 in reactive astrocytes: *in vitro* ERK1/2 activation and role in Alzheimer's disease. *J. Neuroimmunol.* 108, 227–235. doi: 10.1016/S0165-5728(00)00285-X

Xuan, A., Long, D., Li, J., Ji, W., Zhang, M., Hong, L., et al. (2012). Hydrogen sulfide attenuates spatial memory impairment and hippocampal neuroinflammation in β-amyloid rat model of Alzheimer's disease. *J. Neuroinflammation* 9:202. doi: 10.1186/1742-2094-9-202

Yamada, K., Tanaka, T., Han, D., Senzaki, K., Kameyama, T., and Nabeshima, T. (1999). Protective effects of idebenone and alpha-tocopherol on beta-amyloid-(1–42)-induced learning and memory deficits in rats: implication of oxidative stress in beta-amyloid-induced neurotoxicity *in vivo*. *Eur. J. Neurosci.* 11, 83–90. doi: 10.1046/j.1460-9568.1999.00408.x

Yan, J. J., Cho, J. Y., Kim, H. S., Kim, K. L., Jung, J. S., Huh, S. O., et al. (2001). Protection against beta-amyloid peptide toxicity *in vivo* with long-term administration of ferulic acid. *Br. J. Pharmacol.* 133, 89–96. doi: 10.1038/sj.bjp.0704047

Yang, S., Xia, C., Li, S., Du, L., Zhang, L., and Zhou, R. (2014). Defective mitophagy driven by dysregulation of rheb and KIF5B contributes to mitochondrial reactive oxygen species (ROS)-induced nod-like receptor 3 (NLRP3) dependent proinflammatory response and aggravates lipotoxicity. *Redox Biol.* 3, 63–71. doi: 10.1016/j.redox.2014.04.001

Yeung, J. H. Y., Calvo-Flores Guzmán, B., Palpagama, T. H., Ethira, J., Zhai, Y., Tate, W. P., et al. (2020a). Beta amyloid 1–42 ($Aβ_{1–42}$)-induced alterations in glutamate receptor and transporter expression in the mouse hippocampus. *J. Neurochemistry* 155, 62–80. doi: 10.1111/jnc.15099.

Yeung, J. H. Y., Palpagama, T. H., Tate, W. P., Peppercorn, K., Waldvogel, H. J., Faull, R. L. M., et al. (2020b). The acute effects of amyloid-$beta_{(1–42)}$ on glutamatergic receptor and transporter expression in the mouse hippocampus. *Front. Neurosci.* 13:1427. doi: 10.3389/fnins.2019.01427

Yoshiyama, Y., Higuchi, M., Zhang, B., Huang, S. M., Iwata, N., Saido, T. C., et al. (2007). Synapse loss and microglial activation precede tangles in a P301S tauopathy mouse model. *Neuron* 53, 337–351. doi: 10.1016/j.neuron.2007.01.010

Zempel, H., and Mandelkow, E. (2014). Lost after translation: missorting of Tau protein and consequences for Alzheimer disease. *Trends Neurosci.* 37, 721–732. doi: 10.1016/j.tins.2014.08.004

Zhang, L., Fang, Y., Lian, Y., Chen, Y., Wu, T., Zheng, Y., et al. (2015). Brain-derived neurotrophic factor ameliorates learning deficits in a rat model of Alzheimer's disease induced by $Aβ_{1–42}$. *PLoS One* 10:e0122415. doi: 10.1371/journal.pone.0122415

Conflict of Interest: The authors declare that the research was conducted in the absence of any commercial or financial relationships that could be construed as a potential conflict of interest.

Copyright © 2020 Calvo-Flores Guzmán, Chaffey, Palpagama, Waters, Boix, Tate, Peppercorn, Dragunow, Waldvogel, Faull and Kwakowsky. This is an open-access article distributed under the terms of the Creative Commons Attribution License (CC BY). The use, distribution or reproduction in other forums is permitted, provided the original author(s) and the copyright owner(s) are credited and that the original publication in this journal is cited, in accordance with accepted academic practice. No use, distribution or reproduction is permitted which does not comply with these terms.